

Aromatic enriched oil production via microwave-assisted catalytic co-pyrolysis of baked semen abutilon seeds and waste expanded polystyrene

Faizan Ahmad ^a, Yaning Zhang ^{a,*} , Zhihong Liu ^a, Wenke Zhao ^a, Wei Liu ^b, Yong Shuai ^a

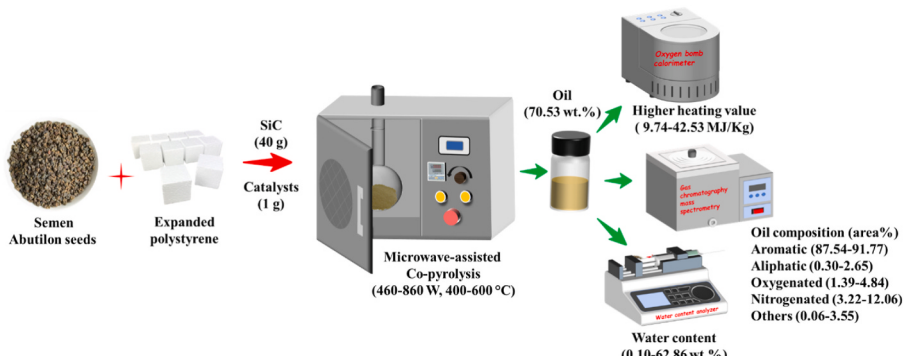
^a School of Energy Science and Engineering, Harbin Institute of Technology, Harbin, 150001, China

^b Heilongjiang Institute of Energy and Environment, Harbin, 150007, China

HIGHLIGHTS

- Co-pyrolysis of SAS and EPS was studied on products and oil composition.
- Optimal oil yield was achieved at 500 °C and 660 W using CaO catalyst.
- CaO catalyst improved the oil yield from 52.05 wt% to 70.53 wt%.
- Catalytic co-pyrolysis enhanced the aromatic hydrocarbons content in the oil.
- CaO and Al₂O₃ catalysts showed a positive synergistic effect on oil production.

GRAPHICAL ABSTRACT



ARTICLE INFO

Keywords:
 Microwave heating
 Catalyst
 Expanded polystyrene
 Semen abutilon seeds
 Oil recovery
 Aromatic hydrocarbons

ABSTRACT

Co-pyrolysis of biomass and plastic waste presents a promising strategy for waste valorization and fuel upgrading. This study explored microwave-assisted co-pyrolysis of expanded polystyrene (EPS) and Semen Abutilon seeds (SAS) using metal oxides (Al₂O₃, CaO), inorganic salts (Na₂CO₃, Fe(NO₃)₃·9H₂O), and zeolite (ZSM-5) as catalysts. The effects of catalyst type, microwave power (460–860 W), and pyrolysis temperature (400–600 °C) on oil yield and composition were evaluated. Using an EPS:SAS blend ratio of 2:1, optimal conditions were identified as 660 W and 500 °C, with CaO emerging as the most effective catalyst, achieving a maximum oil yield (70.53 wt%), thermal efficiency (47.33 %), and recovery efficiency (98.83 %). Compared to non-catalytic pyrolysis (52.02 wt%), CaO and Al₂O₃ increased oil yield by 35.56 % and 25.94 %, respectively, showing positive synergistic effects of 10.13 % and 2.79 %. The use of Fe(NO₃)₃·9H₂O resulted in oil with a high-calorific value (42.53 MJ/kg), while ZSM-5 reduced water content (from 12.60 to 3.37 wt%). Although SAS-derived oil was rich in oxygenated hydrocarbons (74.92 area%), catalytic co-pyrolysis promoted deoxygenation and aromatization reactions, yielding oil high in aromatic hydrocarbons (87.54–91.77 area%). These results confirm SAS and EPS as synergistic feedstocks capable of producing high-quality oils through microwave-assisted co-pyrolysis.

* Corresponding author.

E-mail address: ynzhang@hit.edu.cn (Y. Zhang).

1. Introduction

Expanded polystyrene (EPS) is a synthetic polymer composed of long-chain hydrocarbons with alternating carbon atoms linked to phenyl groups. Due to its lightweight nature and excellent insulating properties, EPS is widely used in packaging, thermal insulation, and construction (Kulakovskaya et al., 2023). The global EPS market, estimated at 12.84 million tons in 2025, is projected to grow at an annual rate of 3.05 %, reaching 14.92 million tons by 2030 (Mordor Intelligence, 2025). However, its non-biodegradable nature leads to severe environmental pollution after disposal, as EPS persists in landfills, breaks down into microplastics, and contaminates ecosystems (Rillig and Lehmann, 2020). This accumulation poses long-term risks to terrestrial and aquatic environments, underscoring the urgent need for sustainable waste management strategies.

Pyrolysis, a thermal degradation process, has emerged as a promising method for converting waste plastics and biomass into valuable oils and gases (Nanda and Berruti, 2021; Ephraim et al., 2018). However, conventional pyrolysis often suffers from high energy consumption, slow reaction rates, and inconsistent product yields, which limit its overall process efficiency (Anshu et al., 2024). In this context, microwave-assisted pyrolysis stands out as a transformative approach, providing rapid and uniform heating, superior energy efficiency, and better control over reaction conditions (Huang et al., 2016). The poor microwave absorbability of both biomass and plastic frequently necessitates the incorporation of microwave absorbers to achieve efficient heating. Carbon-based materials and metal oxides are commonly used for this purpose due to their strong ability to convert microwave energy into heat (Jing et al., 2021). Among these, silicon carbide (SiC) is preferred owing to its cost-effectiveness, exceptional thermal stability, high mechanical strength, and reusability (Duan et al., 2017).

Bio-oil derived from pyrolysis often suffers from poor stability and high viscosity due to the presence of oxygenated compounds, including acids, aldehydes, ketones, furans, and phenols (Dai et al., 2020; Lin et al., 2022a). In contrast, plastic-derived oils primarily consist of aromatic and aliphatic hydrocarbons (Kumar Mishra and Mohanty, 2020), making them a more suitable alternative for petrochemical applications. To enhance the storage stability, energy density, and transportability of pyrolysis oils, upgrading is essential. Among various upgrading methods, co-pyrolysis is particularly effective, as hydrogen-rich plastics compensate for the oxygen-rich nature of biomass, creating a synergistic interaction that improves oil properties. This process not only yields a more fuel-compatible product but also offers a more efficient waste management solution than pyrolysis alone. Numerous studies have investigated the co-pyrolysis of biomass with EPS. For instance, the co-pyrolysis of rice husk and EPS increased aromatic hydrocarbons

dramatically, from 37.80 area% (rice husk alone) and 35.00 area% (EPS alone) to 90.70 area% in combination (Suriapparao et al., 2020). Similarly, blending Mahua seeds with 20.00 wt% EPS increased the aromatic hydrocarbon yield from 12.85 area% to 31.88 area% (Kumar Mishra and Mohanty, 2020). Co-pyrolysis of Karanja seeds, Niger seeds, and EPS enhanced the total oil yield by reducing the formation of non-condensable gases (Shadangi and Mohanty, 2015). Furthermore, co-pyrolysis of sargassum algae with EPS reduced the oxygen content from 9.00 area% to 0.30 area% (Kositkanawuth et al., 2017). Pine sawdust-EPS co-pyrolysis improved the oil quality by decreasing oxygenated compounds from 51.77 area% to 5.04 area% and water content from 18.69 wt% to 0.05 wt% (Van Nguyen et al., 2019). Co-pyrolysis of pine needles with EPS lowered the apparent activation energy compared to biomass alone (Varma et al., 2021). Poplar wood co-pyrolysis with polystyrene revealed synergistic interactions through discrepancies between calculated and experimental values (Ephraim et al., 2018). The synergistic effects of co-pyrolysis also improve the calorific value of the resulting oils, making them better suited for blending with conventional fuels.

Catalytic upgrading can further enhance co-pyrolysis efficiency by improving selectivity towards desirable hydrocarbons. Catalyst choice depends on the composition of initial pyrolysis products and the target compounds to be enhanced. Calcium oxide (CaO) has proven effective in EPS-coffee grounds co-pyrolysis, facilitating EPS degradation to generate hydrogen-rich fragments that drive Diels-Alder and hydrogen transfer reactions, while reducing oxygenates such as aldehydes and acids (Van Nguyen et al., 2024). Moreover, CaO is known for its capacity to capture CO₂ and mitigate tar formation (Wang et al., 2020). On the other hand, zeolite catalysts, particularly ZSM-5, play a different role in catalytic co-pyrolysis. In microwave-assisted co-pyrolysis of EPS and algae, the acidic sites of ZSM-5 facilitated conversion of phenols, furans, and acids into aromatics, improving the oil's calorific value while reducing viscosity, density, and flash point (Suriapparao et al., 2022). However, ZSM-5's strong acidity can lead to excessive cracking, increasing non-condensable gases formation and reducing overall oil yield. A similar trend was observed during the co-pyrolysis of bagasse with polystyrene, where ZSM-5 enhanced aromatic yield but decreased total oil yield. This is attributed to its high BET and Langmuir surface area, along with high micro-porosity, which promoted excessive secondary cracking (Iftikhar et al., 2019).

Although previous studies have investigated the co-pyrolysis of EPS with various biomass resources, Semen Abutilon seeds have yet to be explored in this context. Semen Abutilon, a fast-growing herbaceous plant belonging to the Malvaceae family, is commonly found in warm-temperate and subtropical regions, with annual production in China reaching around 20,000 tons (Sun et al., 2021). Its seeds hold significant

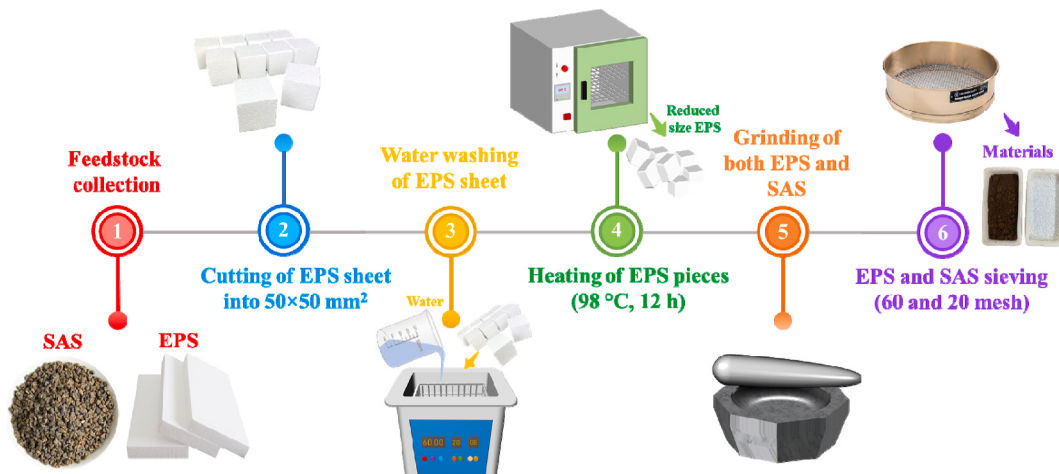


Fig. 1. Feedstock processing flow diagram for microwave-assisted co-pyrolysis.

Table 1
Proximate and ultimate analysis of the feedstock.

Material	Expanded polystyrene	Semen Abutilon seed
Proximate analysis (wt%) ^{db}		
Moisture	0.02	4.69 ± 0.03
Ash	0.90 ± 0.04	15.75 ± 0.26
Volatiles	98.88 ± 0.95	67.92 ± 1.92
Fixed carbon ^a	0.19 ± 0.01	11.63 ± 0.67
Ultimate analysis (wt%)		
Carbon	90.88	48.67
Oxygen ^a	1.84	41.27
Hydrogen	7.23	6.14
Nitrogen	0.05	3.90
Sulfur	0.00	0.02
HHV (MJ/kg)	40.53 ± 0.87	19.30 ± 0.63

Note: ^{db} stands for dry basis; ^a stands for calculation by differences.

potential as a pyrolysis feedstock for oil production. Despite this promise, the co-pyrolysis potential of Semen Abutilon seeds with EPS remains entirely unexplored, highlighting a gap in the research literature.

Hence, the current study investigates the microwave-assisted co-pyrolysis of Semen Abutilon seeds and expanded polystyrene, focusing on the influence of catalysts on product selectivity toward aromatic hydrocarbons. The objectives are to: (a) assess the feasibility of oil recovery from Semen Abutilon seeds; (b) examine the effects of catalysts, pyrolysis temperatures (400–600 °C), and microwave power (460–860 W) on product distribution (oil, syngas, and residue), oil composition, and the efficiencies (thermal, recovery, and conversion) of the co-pyrolysis process; and (c) characterize the resulting oil by analyzing its chemical composition, water content, and higher heating values.

2. Materials and methods

2.1. Materials

Baked Semen Abutilon seeds (SAS), sourced from Qingdao International Seed Co., Ltd. (China), were used as the biomass feedstock. The seeds were pale brown, heart-shaped, and measured approximately 3.4–4 mm in length and 3 mm in width. EPS, collected from the logistics market at Harbin Institute of Technology, China, served as the plastic feedstock. The EPS foam was cut into 50 mm × 50 mm × 35 mm (length × width × thickness) pieces, rinsed with distilled water for 2–3 min to remove surface contaminants, and then oven-dried at 98 °C for 12 h. After drying, the EPS sheets shrank by 40–50 % and became rigid. The SAS particles were passed through a 60-mesh screen, resulting in a particle size of ~0.25 mm, while the EPS particles were sieved through a

20-mesh screen, resulting in a particle size of ~0.841 mm, as per standard sieve conversions. The feedstock processing steps are illustrated in Fig. 1, and results of the proximate and ultimate analyses results are summarized in Table 1. The proximate analysis of the biomass followed the GB/T 212–2008 standard, and the ultimate analysis (elemental composition) was performed using a Vario EL III analyzer (Elementar, Germany).

Due to the low microwave absorption capability of the feedstocks, irregularly shaped SiC particles with sizes ranging from 2 to 3 mm were employed as microwave absorbers. In this study, five catalysts were utilized, including sodium carbonate (Na_2CO_3), aluminum oxide (Al_2O_3), calcium oxide (CaO), universal zeolite (ZSM-5), and iron (III) nitrate nonahydrate [$\text{Fe}(\text{NO}_3)_3 \cdot 9\text{H}_2\text{O}$]. These catalysts were purchased from Senow Chemical Co., Ltd. (China) as fine powders.

2.2. Experimental system

The microwave-assisted co-pyrolysis apparatus, illustrated in Fig. 2, includes the following components: (1) microwave oven, (2) quartz reactor, (3) K-type thermocouple, (4) temperature display, (5) electricity meter, (6) cooling system, (7) cooling bath, (8) vacuum pump, and (9) blower.

A laboratory microwave oven (Donlim Weili Electrical Appliances Co., Ltd., China), operating at 2450 MHz, was employed as the primary heat source for pyrolysis. The pyrolysis reaction was conducted in a 150 mL quartz glass reactor, ensuring a stable and controlled environment. Temperature monitoring was achieved using a K-type thermocouple (Jiangsu Shazi Electric Appliance Co., Ltd., China) connected to a digital thermometer (TA612C, TASI Test and Automation Co., Ltd., China) with a measurement range of up to 1000 °C and an accuracy of ±0.1 °C. The electricity consumption of the microwave oven was recorded using an electricity meter (UT230A-II, Uni-Trend Technology Co., Ltd., China). For vapor condensation, the pyrolysis system incorporated a cooling system consisting of connecting tubes submerged in a cooling bath. A vacuum pump maintained an oxygen-free environment within the reaction system, while a blower was used to prevent the syngas accumulation in the experimental workspace.

2.3. Experimental procedure

Before the final experimental design, preliminary screening tests were conducted across different parametric combinations of microwave power, pyrolysis temperature, and catalyst loading. These exploratory experiments showed that optimal oil yields were achieved at 500 °C, 660 W, and 1 g catalyst loading, which were then selected as baseline conditions for the subsequent final investigation.

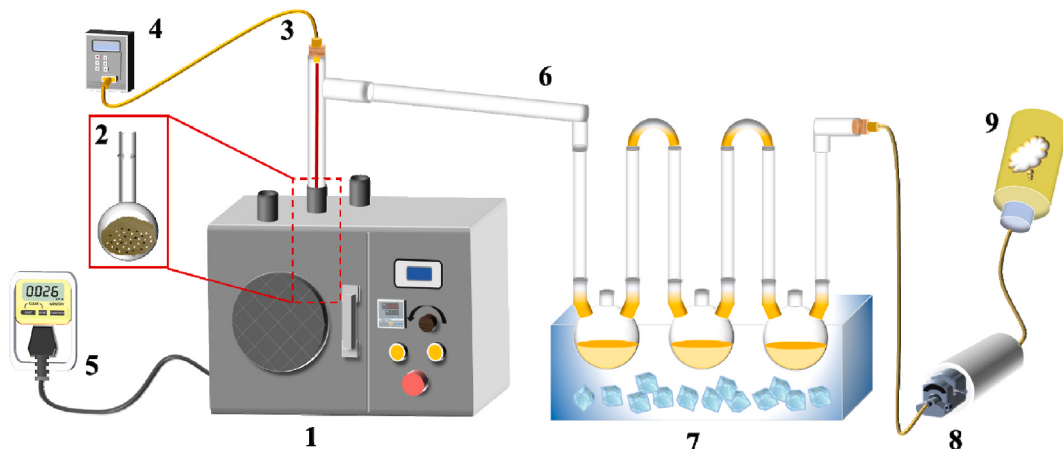


Fig. 2. Schematic diagram of the experimental system for microwave co-pyrolysis: (1) microwave oven, (2) quartz reactor, (3) K-type thermocouple, (4) digital thermometer, (5) electricity meter, (6) cooling system, (7) cooling bath, (8) vacuum pump, and (9) blower.

Table 2

Experimental design for microwave-assisted catalytic co-pyrolysis process.

Code	EPS: SAS	Catalyst (1 g)	Temperature (°C)	Microwave power (W)
E ₁	0:1	–	500	660
E ₂	1:2	–	500	660
E ₃	1:1	–	500	660
E ₄	2:1	–	500	660
E ₅	1:0	–	500	660
E ₆	2:1	Na ₂ CO ₃	500	660
E ₇	2:1	Al ₂ O ₃	500	660
E ₈	2:1	CaO	500	660
E ₉	2:1	ZSM-5	500	660
E ₁₀	2:1	Fe (NO ₃) ₃ ·9H ₂ O	500	660
E ₁₁	2:1	CaO	400	660
E ₁₂	2:1	CaO	450	660
E ₁₃	2:1	CaO	550	660
E ₁₄	2:1	CaO	600	660
E ₁₅	2:1	CaO	500	460
E ₁₆	2:1	CaO	500	560
E ₁₇	2:1	CaO	500	760
E ₁₈	2:1	CaO	500	860

In the final investigation, the study first examined the individual pyrolysis of EPS (0:1) and SAS (1:0), followed by co-pyrolysis at intermediate blend ratios (1:2, 1:1, and 2:1) to assess potential synergistic interactions. The EPS:SAS blend ratio of 2:1 demonstrated the most favorable synergy in terms of oil yield and was thus selected for subsequent experiments. Using the optimized blend (2:1), the effect of catalyst type was investigated at a fixed pyrolysis temperature (500 °C) and microwave power (610 W). Among the tested catalysts, CaO exhibited the highest catalytic activity and was selected for further studies on the effects of microwave power and pyrolysis temperature. A detailed summary of experimental parameters is provided in Table 2, with discussions of process conditions presented in Sections 3.4–3.6.

For each experiment, a homogeneous mixture was prepared by blending 20 g of feedstock with 40 g of SiC (as a microwave absorber) and 1 g of catalyst (see Table 2 for specific compositions). Prior to pyrolysis, the quartz reactor, thermocouple, and cooling unit were weighed and recorded. The prepared mixture was then transferred into a 150 mL quartz reactor and placed inside the microwave oven cavity. A thermocouple was inserted into the quartz reactor to monitor temperature, while the cooling unit and auxiliary components were assembled as shown in Fig. 2. To minimize heat dissipation, the microwave oven cavity was insulated with quartz wool, and all joints were securely clamped to prevent syngas leaks and air ingress. The system was purged of oxygen by evacuating it with a vacuum pump for 8 min. Pyrolysis was then initiated by setting the microwave oven to the target microwave power (see Table 2). The SiC particles efficiently absorbed microwave energy, converting it into heat and increasing the feedstock temperature. Upon reaching the desired pyrolysis temperature, the microwave oven was deactivated to prevent overheating and then promptly reactivated (after 1–2 s) to maintain the set pyrolysis temperature. This intermittent cycling ensured that the temperature remained within ±12 °C of the target throughout the experiment. During pyrolysis, feedstock decomposed into volatile vapors, which partially condensed in the cooling unit to form oil, while non-condensable gases were evacuated from the system. The microwave operation was terminated once vapor evolution ceased (as observed by real-time visual monitoring), marking the completion of pyrolysis. Each experiment lasted 20–30 min and was repeated at least twice to ensure reproducibility.

After completion of the pyrolysis experiments, the quartz reactor and cooling system were reweighed. The oil yield was calculated from the weight difference of the thermocouple and cooling system before and after the experiments, while the residue yield was determined from the weight difference of the quartz reactor before and after the experiments. Any remaining products, excluding oil and residue, were classified as

syngas yield.

2.4. Data evaluation

The oil, syngas, and residue yields obtained from the co-pyrolysis experiment were calculated using Equations (1)–(5), respectively.

$$m_{\text{oil}} = m_{c'} - m_{c''} + m_{t'} - m_{t''} \quad (1)$$

$$Y_{\text{oil}} = \frac{m_{\text{oil}}}{m_{\text{feedstock}}} \times 100\% \quad (2)$$

$$m_{\text{residue}} = m_{q'} - m_{q''} - m_{\text{SiC}} \quad (3)$$

$$Y_{\text{residue}} = \frac{m_{\text{residue}}}{m_{\text{feedstock}}} \times 100\% \quad (4)$$

$$Y_{\text{syngas}} = 100\% - Y_{\text{oil}} - Y_{\text{residue}} \quad (5)$$

where:

Y_{oil}	is the oil yield, wt%
Y_{residue}	is the residue yield, wt%
Y_{syngas}	is the syngas yield, wt%
m_{oil}	is the mass of oil, wt%
m_{residue}	is the amount of residue obtained from the experiment, g
$m_{\text{feedstock}}$	is the amount of feedstock used in the experiment, g
m_{SiC}	is the mass of silicon carbide used in experiment, g
$m_{c'}$	is the weight of cooling unit before the experiment, g
$m_{c''}$	is the weight of cooling unit after the experiment, g
$m_{t'}$	is the weight of thermocouple before the experiment, g
$m_{t''}$	is the weight of thermocouple after the experiment, g

The synergistic effect between the plastic and biomass is quantified by comparing the experimental results with the theoretical results, which were calculated using Equations (6) and (7) (Stančin et al., 2022).

$$Y_{\text{the}} = (X_{\text{EPS}} \times Y_{\text{EPS}}) + (X_{\text{SAS}} \times Y_{\text{SAS}}) \quad (6)$$

$$\Delta Y = \frac{Y_{\text{exp}} - Y_{\text{the}}}{Y_{\text{the}}} \times 100\% \quad (7)$$

where:

Y_{the}	is the theoretical yield, wt%
Y_{exp}	is the experimental yield, wt%
ΔY	is the synergistic effect, %
X_{EPS}	is the mass fraction of expanded polystyrene in the feedstock, %
Y_{EPS}	is the oil yield obtained from the pyrolysis of expanded polystyrene, wt%
X_{SAS}	is mass fraction of Semen Abutilon seeds in the feedstock, %
Y_{SAS}	is the oil yield obtained from the Semen Abutilon seeds, wt%.

In the co-pyrolysis experiments, the involved energy was categorized into input energy and output energy. The input energy consisted of the energy contained in the feedstock and the electrical energy (W_{in}) supplied to the microwave oven for operation. The output energy corresponds to the energy present in the produced oil. The electricity consumed by the microwave oven was measured using an electricity meter. The energy in the feedstock and oil were calculated using Equations (8) and (9). The higher heating values (HHVs) of both oil and feedstock were determined using an oxygen bomb calorimeter.

The performance of the co-pyrolysis process was evaluated by calculating the thermal efficiency, recovery efficiency, and conversion efficiency using Equations (10)–(12) (Suriapparao et al., 2020).

$$Q_{\text{oil}} = m_{\text{oil}} \times HHV_{\text{oil}} \quad (8)$$

$$Q_{\text{feedstock}} = m_{\text{feedstock}} \times HHV_{\text{feedstock}} \quad (9)$$

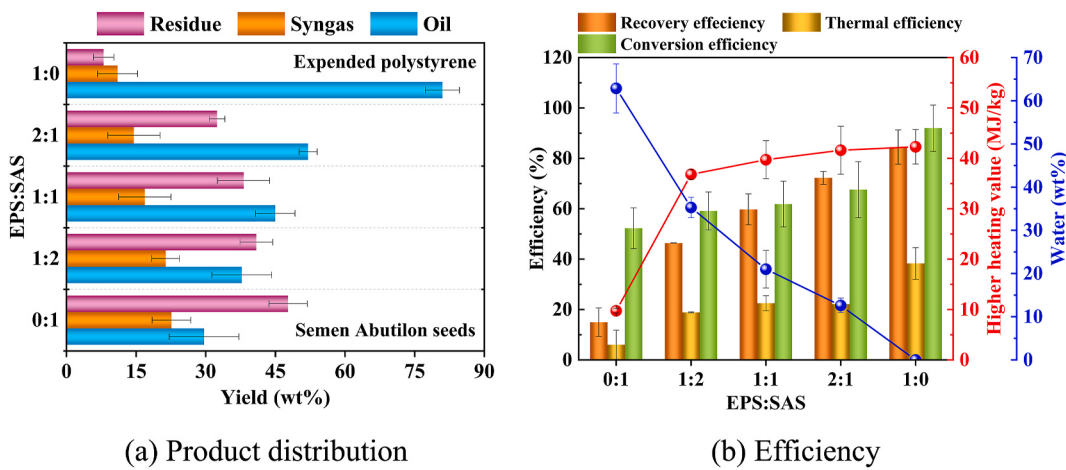


Fig. 3. Results obtained from co-pyrolysis of expanded polystyrene and Semen Abutilon seeds at different blend ratios.

$$\eta_T = \frac{Q_{\text{oil}}}{Q_{\text{feedstock}} + W_{\text{in}}} \times 100\% \quad (10)$$

$$\eta_R = \frac{Q_{\text{oil}}}{Q_{\text{feedstock}}} \times 100\% \quad (11)$$

$$\eta_C = 100\% - Y_{\text{residue}} \quad (12)$$

where:

Q_{oil}	is the energy of oil, J
$Q_{\text{feedstock}}$	is the energy of feedstock, J
HHV_{oil}	is the higher heating value of oil, J/g
$HHV_{\text{feedstock}}$	is the higher heating value of feedstock, J/g
W_{in}	is the input electric energy used by microwave oven, J
η_T	is the thermal efficiency, %
η_R	is the recovery efficiency, %
η_C	is the conversion efficiency, %.

The water content in the oil was measured using a trace moisture analyzer (HD-JJWS2, Shandong Holder Electronic Technology Co., Ltd., China) based on the Karl Fischer titration principle.

The oil's chemical constituents were characterized using an Agilent 7890 gas chromatography-mass spectrometry (GC-MS) system, equipped with a 5977 A mass selective detector. Separation was performed on a 30 m × 0.25 mm HP-5MS capillary column coated with a 0.25 μm stationary phase. The temperature program started with an initial 2-min hold at 50 °C, then increased at 5 °C per minute until reaching 300 °C, with a final 10-min hold to elute heavier components. Samples (1 μL) were introduced through a 280 °C splitless injector, with helium as the carrier gas at a constant flow of 1.0 mL/min. The mass spectrometer employed 70 eV electron impact ionization, with the source and analyzer maintained at 230 °C and 150 °C, respectively. A mass range of 50–500 amu was scanned for comprehensive detection. Compound quantification relied on normalized peak areas from the total ion current, while identification was performed by matching acquired spectra against the NIST reference library.

3. Results and discussion

3.1. Microwave-assisted co-pyrolysis of EPS and SAS

The yields of oil, syngas, and residue obtained from co-pyrolysis of EPS and SAS at different blend ratios are presented in Fig. 3 (a). As the EPS:SAS ratio increased from 0:1 to 1:0, the oil yield increased continuously from 29.64 to 80.97 wt%, while the syngas and residue yields decreased from 22.60 to 10.99 wt% and 47.74 to 8.02 wt%, respectively.

Notably, the oil yield from EPS pyrolysis (80.97 wt%) exceeded those reported in previous studies for both thermal pyrolysis (Calero et al., 2023; Van Nguyen et al., 2021) and microwave pyrolysis (Kachhadia et al., 2023; Suriapparao et al., 2022). In contrast, SAS biomass yielded only 29.64 wt% oil, with significant char formation attributed to its low volatile matter and high ash content (Table 1). As the EPS proportion increased, the oil yield improved, with a maximum yield of 52.05 wt% observed at a 2:1 blend ratio. This synergistic improvement aligns with findings from previous co-pyrolysis study (Stancin et al., 2022). This improvement can be attributed to the polymeric nature of EPS, high carbon content (90.88 wt%) (Calero et al., 2023), and hydrogen-rich composition. The high carbon content facilitated the formation of condensable vapors rather than syngas (Kachhadia et al., 2023), while the hydrogen atoms helped stabilize free radicals from SAS decomposition (Yu et al., 2019), reducing secondary reactions and minimizing residue formation.

The process efficiencies, higher heating values (HHVs), and water content obtained at different blend ratios are presented in Fig. 3 (b). As the ratio shifted from 1:0 to 0:1, both process efficiencies and HHVs showed a consistent increase, while the water content in the oil decreased. Notably, the oil derived from EPS contained no water, whereas SAS-derived oil had a higher water content (62.86 wt%). The HHV of EPS-derived oil (42.28 MJ/kg) far exceeded that of SAS-derived oil (9.74 MJ/kg), reflecting the superior energy density of the plastic-derived product. Increasing the plastic proportion improved oil quality by simultaneously reducing moisture and enhancing calorific value (Sebestyén et al., 2017; Sridevi et al., 2022). Thermal and recovery efficiencies, which depend on both oil yield and HHV, ranged from 6.02 % to 38.31 % and 14.96 %–84.48 %, respectively.

3.2. Effect of catalyst on the co-pyrolysis process

The effect of the catalyst on the co-pyrolysis of EPS and SAS was investigated using Na₂CO₃, Al₂O₃, CaO, ZSM-5, and Fe(NO₃)₃·9H₂O. The catalytic co-pyrolysis experiments were conducted with an EPS:SAS blend ratio of 2:1 at a constant microwave power of 660 W, the catalysts amount of 1 g, and a pyrolysis temperature of 500 °C. The results obtained from the effect of catalysts on microwave-assisted co-pyrolysis of EPS and SAS are presented in Fig. 4.

The oil, syngas, and residue yields obtained from the catalytic co-pyrolysis are presented in Fig. 4 (a). The metal oxide catalysts (Al₂O₃ and CaO) showed superior performance, increasing oil yields from 52.05 wt% (non-catalytic) to 70.53 wt% and 65.83 wt%, respectively. In contrast, Na₂CO₃, ZSM-5, and Fe(NO₃)₃·9H₂O catalysts showed slightly lower oil yields of 49.79 wt%, 51.25 wt%, and 49.50 wt%, respectively. The reduced oil yield may be attributed to: (a) catalyst deactivation

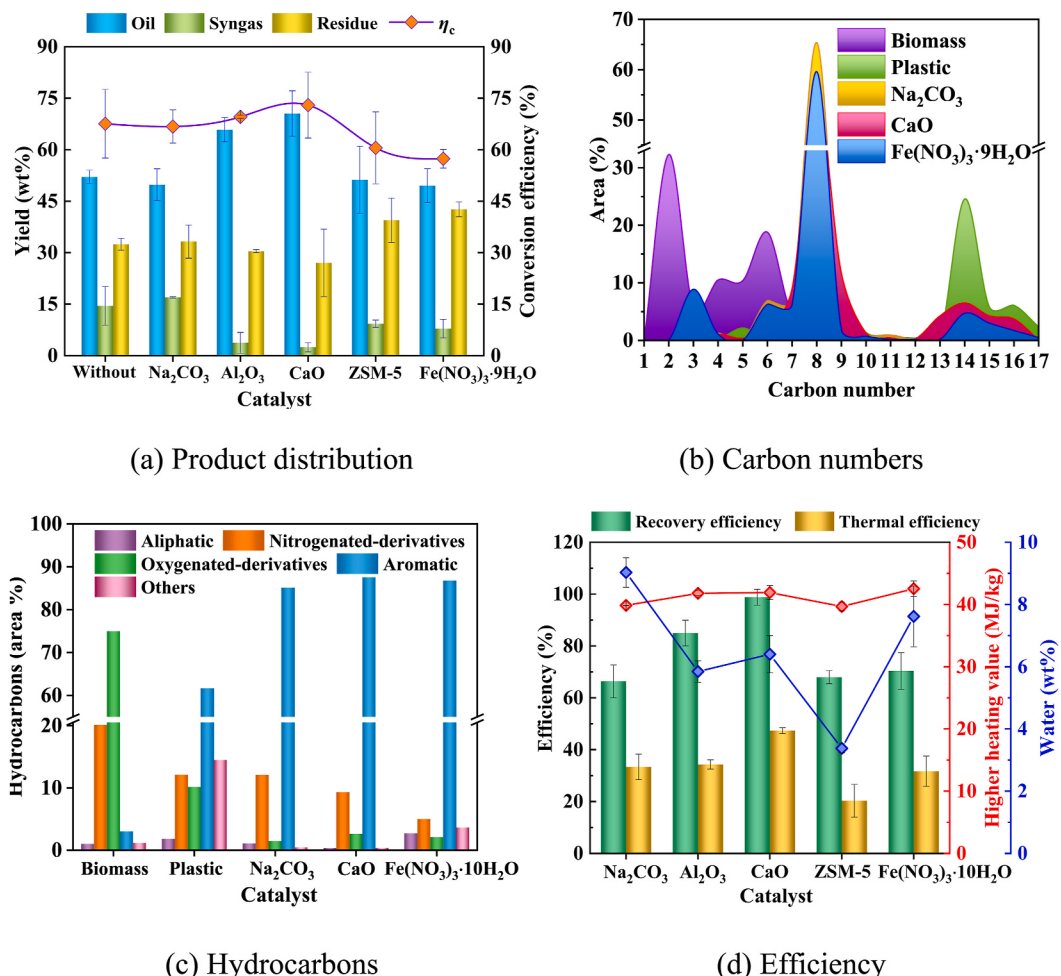


Fig. 4. Effect of different catalysts on microwave-assisted co-pyrolysis of expanded polystyrene and Semen Abutilon seeds.

through coke deposition, sintering, or active site poisoning (Lin et al., 2022a; Ochoa et al., 2020); (b) enhanced secondary reactions promoting lighter hydrocarbons and non-condensable gas formation (Sebestyén et al., 2017); (c) limited feedstock-catalyst synergy, where preferential decomposition of one feedstock component led to imbalanced product distribution (Sridevi et al., 2022); and (d) insufficient catalyst loading, potentially restricting catalytic efficacy (Duan et al., 2017; Pan et al., 2023).

The choice of catalyst influenced pyrolysis behavior through distinct mechanistic controls. In CaO-catalyzed co-pyrolysis, real-time (visual) monitoring revealed a characteristic two-phase vapor generation. The initial phase corresponded to feedstock thermal degradation, while the secondary phase (occurring 5–7 min later) involved tar cracking and conversion of unconverted biomass into lighter hydrocarbons (Pan et al., 2023; Wang et al., 2022). This biphasic behavior aligns with the decomposition mechanisms reported by Yu et al. (2019), wherein primary oils form through the co-decomposition of cellulose, hemicellulose, and plastic components in the first phase, while secondary oils result from the subsequent degradation of remaining plastic residues and lignin in the second phase. Similar observations by Tian et al. (2021) revealed initial weak bond dissociation in biomass constituents preceding extensive cracking in the second phase. Additionally, CaO enhanced biomass dehydration during the early stages of pyrolysis due to its hygroscopic nature (Wang et al., 2020). By adsorbing moisture, CaO minimized condensate formation in cooling systems, thereby improving oil quality. In contrast, ZSM-5 showed better cracking efficiency, causing rapid feedstock decomposition at lower temperatures. This led to faster vapor release and a shorter overall pyrolysis duration,

consistent with the findings of Sebestyén et al. (2017), who attributed this effect to the acidic sites of the zeolite that enhance bond scission and reduce thermal degradation thresholds. While these acidic sites improve selectivity toward desirable compounds, they also promote coke formation due to excessive secondary reactions (Iliopoulou et al., 2012). Meanwhile, $\text{Fe}(\text{NO}_3)_3 \cdot 9\text{H}_2\text{O}$ catalyzed pyrolysis produced brown gases that condensed into a dark brown bio-oil, leaving a black ash (residue) in the quartz reactor.

The carbon composition of oil produced from the co-pyrolysis process, both uncatalyzed and catalyzed by Na_2CO_3 , CaO, and $\text{Fe}(\text{NO}_3)_3 \cdot 9\text{H}_2\text{O}$, is presented in Fig. 4 (b). SAS-derived oil was primarily composed of low carbon-number hydrocarbons (C_2 – C_8), accounting for 91.70 area% of the total oil. The distribution followed the order: C_2 (33.29 area%) > C_6 (18.81 area%) > C_4 (10.47 area%) > C_5 (10.38 area%) > C_8 (9.23 area%) > C_3 (5.60 area%) > C_7 (4.89 area%) > C_{14} (2.03 area%) > C_{13} (1.45 area%). In contrast, EPS-derived oil was dominated by higher carbon numbers (C_7 – C_9 and C_{14} – C_{16}), with C_8 being the most abundant (38.65 area%), followed by C_{14} (24.56 area%), C_9 (7.31 area%), C_{16} (6.07 area%), C_{15} (5.84 area%), C_7 (4.59 area%), and C_{17} (2.34 area%). The addition of catalysts altered the carbon number distribution (Fig. 4 b), enhancing C_8 hydrocarbons while reducing C_2 hydrocarbons. Specifically, $\text{Fe}(\text{NO}_3)_3 \cdot 9\text{H}_2\text{O}$ catalyst increased C_8 hydrocarbons to 59.60 area%, with other major distributions including C_3 (8.85 area%), C_6 (6.28 area%), C_7 (6.18 area%), and C_{14} (4.69 area%). The CaO showed a similar trend, boosting C_8 to 54.42 area% while nearly eliminating C_2 (0.018 area%). The most pronounced effect was observed with Na_2CO_3 , which maximized C_8 selectivity to 65.38 area%, followed by C_7 (6.89 area%), C_6 (6.78 area%), and C_{14} (5.14 area%).

Table 3

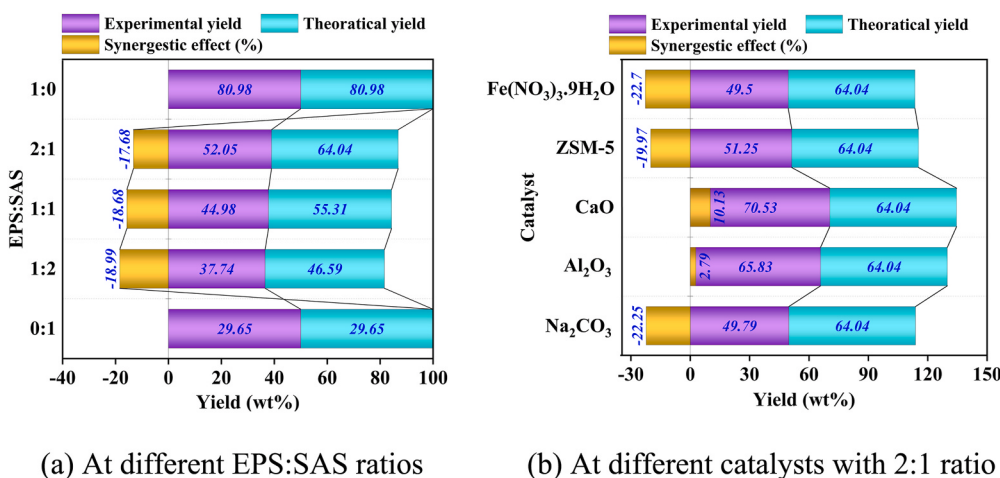
Chemical composition of oil at different catalysts.

Oil component	Formula	Amount (area %)				
		SAS	EPS	Na ₂ CO ₃	CaO	Fe(NO ₃) ₃ ·H ₂ O
Aromatic hydrocarbons						
Benzene	C ₆ H ₆	—	0.42	0.22	0.98	0.92
Toluene	C ₇ H ₈	—	4.55	5.49	8.86	6.72
Styrene	C ₈ H ₈	—	36.64	54.83	42.68	54.34
α-Methylstyrene	C ₉ H ₁₀	—	5.63	5.29	8.07	5.88
Benzene, (1-methylethyl)-	C ₉ H ₁₂	—	0.11	0.39	0.62	0.42
Benzene, 1-propenyl-	C ₉ H ₁₀	—	1.42	0.17	1.00	0.68
Naphthalene	C ₁₀ H ₈	—	0.29	0.02	0.40	0.22
Anthracene	C ₁₄ H ₁₀	—	0.25	—	0.46	0.17
Bibenzyl	C ₁₄ H ₁₄	—	2.77	0.92	0.92	0.79
(E)-Stilbene	C ₁₄ H ₁₂	—	0.42	0.20	0.79	0.43
1H-indene, 2-phenyl-	C ₁₅ H ₁₂	—	0.16	0.07	0.39	0.19
1,3-Diphenylpropane	C ₁₅ H ₁₆	—	0.19	—	1.22	—
Aliphatic hydrocarbons						
1-Heptene	C ₇ H ₁₄	—	—	0.03	0.05	0.02
Undecane	C ₁₁ H ₂₄	—	—	0.02	0.02	0.01
Dodecane	C ₁₂ H ₂₆	—	—	0.03	0.02	—
Tetradecane	C ₁₄ H ₃₀	—	—	0.02	0.04	0.02
Oxygenated derivatives of hydrocarbons						
Ethyl acetate	C ₄ H ₈ O ₂	—	—	0.77	0.93	1.02
Acetic acid, butyl ester	C ₆ H ₁₂ O ₂	—	—	0.24	0.33	0.38
1,2-Propanediol, 3-benzyloxy-1,2-diacetyl-	C ₁₄ H ₁₈ O ₅	—	9.22	0.06	—	0.04
Nitrogenated derivatives of hydrocarbons						
Pyridine	C ₅ H ₅ N	1.17	—	—	0.04	0.02
Methsuximide	C ₁₂ H ₁₃ NO ₂	—	0.19	0.05	0.04	0.02
Hexadecanamide	C ₁₆ H ₃₃ NO	—	—	0.02	0.03	0.03
2,3-Diazabicyclo [2.2.1]hept-2-en, 1,4-diphenyl-	C ₁₇ H ₁₆ N ₂	—	1.25	0.31	0.59	0.26
Others	—	1.08	14.46	0.40	0.33	3.55
4,4'-Bis(tetrahydrothiopyran)	C ₁₀ H ₁₈ S ₂	—	0.01	—	0.01	—
(2,3-diphenylcyclopropyl)methyl phenyl sulfoxide	C ₂₂ H ₂₀ OS	—	1.63	—	0.01	3.45

Fig. 4 (c) presents the major hydrocarbon groups present in oil at different catalysts, with detailed subcomponents listed in Table 3. Four primary hydrocarbon categories were identified, among which aromatic hydrocarbons (2.97–87.54 area%) were the most dominant. EPS-derived oil exhibited a higher proportion of aromatics (61.55 area%) compared to SAS-derived oil (2.97 area%), owing to its styrene-based structure. (Fan et al., 2023; Van Nguyen et al., 2021). The aromatic fraction of EPS-derived oil was dominated by styrene (36.64 area%), α-methylstyrene (5.63 area%), toluene (4.55 area%), and ethylbenzene (2.04 area%), consistent with the polystyrene-derived aromatic profile reported in previous studies (Park et al., 2020; Nanda and Berruti, 2021). Catalytic upgrading with CaO further increased the aromatic concentration to 87.54 area%, likely due to enhanced decarboxylation, deacidification, and aromatization reactions (Kumagai et al., 2018; Tian et al., 2022; Wang et al., 2020).

Oxygenated derivatives constituted the second most abundant hydrocarbon group (Fig. 4 c), with the highest concentration in SAS-derived oil (74.92 area%) due to the inherent oxygen content in biomass (Table 1). The oxygenated fraction in SAS-derived oil comprised acids (35.24 area%), ketones (30.40 area%), alcohols (4.04 area%), and aldehydes (1.25 area%), with acetic acid (22.24 area%) being the predominant component. Catalytic co-pyrolysis effectively reduced oxygenates, a key phenomenon of the co-pyrolysis process (Iftikhar et al., 2019). EPS-derived oil contained a lower concentration of oxygenated derivatives (10.13 area%), of which 1,2-propanediol, 3-benzyloxy-1,2-diacetyl accounted for 9.22 area%. These findings are consistent with the previous study (Adnan et al., 2015), which identified similar oxygenated derivatives during the pyrolysis of polystyrene.

Nitrogenated derivatives ranked as the third most abundant group in the oils (Fig. 4 c), following the order: biomass-derived (20.04 area%) >



(a) At different EPS:SAS ratios

(b) At different catalysts with 2:1 ratio

Fig. 5. Synergistic effect on oil yield during co-pyrolysis of expanded polystyrene and Semen Abutilon seeds.

Table 4

Effect of catalyst on synergistic enhancement of hydrocarbons.

Hydrocarbon	Na ₂ CO ₃ (%)			CaO (%)			Fe(NO ₃) ₃ ·9H ₂ O (%)		
	Y _{exp}	Y _{the}	ΔY	Y _{exp}	Y _{the}	ΔY	Y _{exp}	Y _{the}	ΔY
Aromatic	85.09	42.21	101.54	87.54	42.21	107.34	86.75	42.21	105.47
Aliphatic	1.02	1.52	-33.01	0.30	1.52	-80.29	2.65	1.52	74.03
Nitrogenated-derivative	12.03	14.70	-18.16	9.26	14.70	-37.00	4.96	14.70	-66.25
Oxygenated-derivative	1.39	31.51	-95.58	2.55	31.51	-91.90	2.06	31.51	-93.46
Others	0.4	10.04	-96.01	0.33	10.04	-96.71	3.55	10.04	-64.65

plastic-derived (12.07 area%) > catalytic (4.96–12.06 area%) (Table 3). The SAS-derived oil was dominated by amines (8.45 area%) and amides (2.14 area%), while the EPS-derived oil primarily contained nitrogenated derivatives bound to aromatic hydrocarbons. Notably, Fe (NO₃)₃·9H₂O was the most effective catalyst for reducing nitrogenated derivatives. Aliphatic hydrocarbons were the least abundant (0.30–2.65 area%), mainly comprising higher carbon-number hydrocarbons such as 1-heptene, undecane, dodecane, and tetradecane. However, catalysts did not effectively enhance their concentration in the oil.

The process efficiencies, HHVs, and water content of the oil obtained using different catalysts are presented in Fig. 4 (d). The thermal efficiency and recovery efficiency ranged from 20.28 % to 47.33 % and 66.35 %–98.83 %, respectively, with CaO showing optimal performance. These efficiencies strongly correlated with both oil yield and HHV, where CaO maximized oil production, thereby enhancing overall process efficiency. The highest HHV (42.53 MJ/kg) was achieved with Fe(NO₃)₃·9H₂O, followed by CaO (41.92 MJ/kg), Al₂O₃ (41.80 MJ/kg),

Na₂CO₃ (39.86 MJ/kg), and ZSM-5 (39.67 MJ/kg). The ZSM-5 showed a high-water reduction capability, reducing water content from 12.60 wt % (non-catalytic condition, Fig. 3 b) to 3.37 wt% due to its high surface area and porous structure, which enhanced water adsorption and promoted dehydration reactions (Iliopoulou et al., 2012). For other catalysts, water content decreased as follows: Na₂CO₃ (9.03 wt%) > Fe (NO₃)₃·9H₂O (7.61 wt%) > CaO (6.40 wt%) > Al₂O₃ (5.84 wt%).

3.3. Synergistic effect

In this study, negative synergistic effects on oil yield were observed at different EPS:SAS ratios, as shown in Fig. 5 (a). For the pyrolysis of individual feedstocks (EPS and SAS), the theoretical and experimental oil yields aligned perfectly, resulting in a synergy level (ΔY) of zero. The negative synergy during co-pyrolysis can be attributed to differences in the thermal degradation processes, microwave absorption capabilities, and fuel characteristics of the feedstock (Shadangi and Mohanty, 2015;

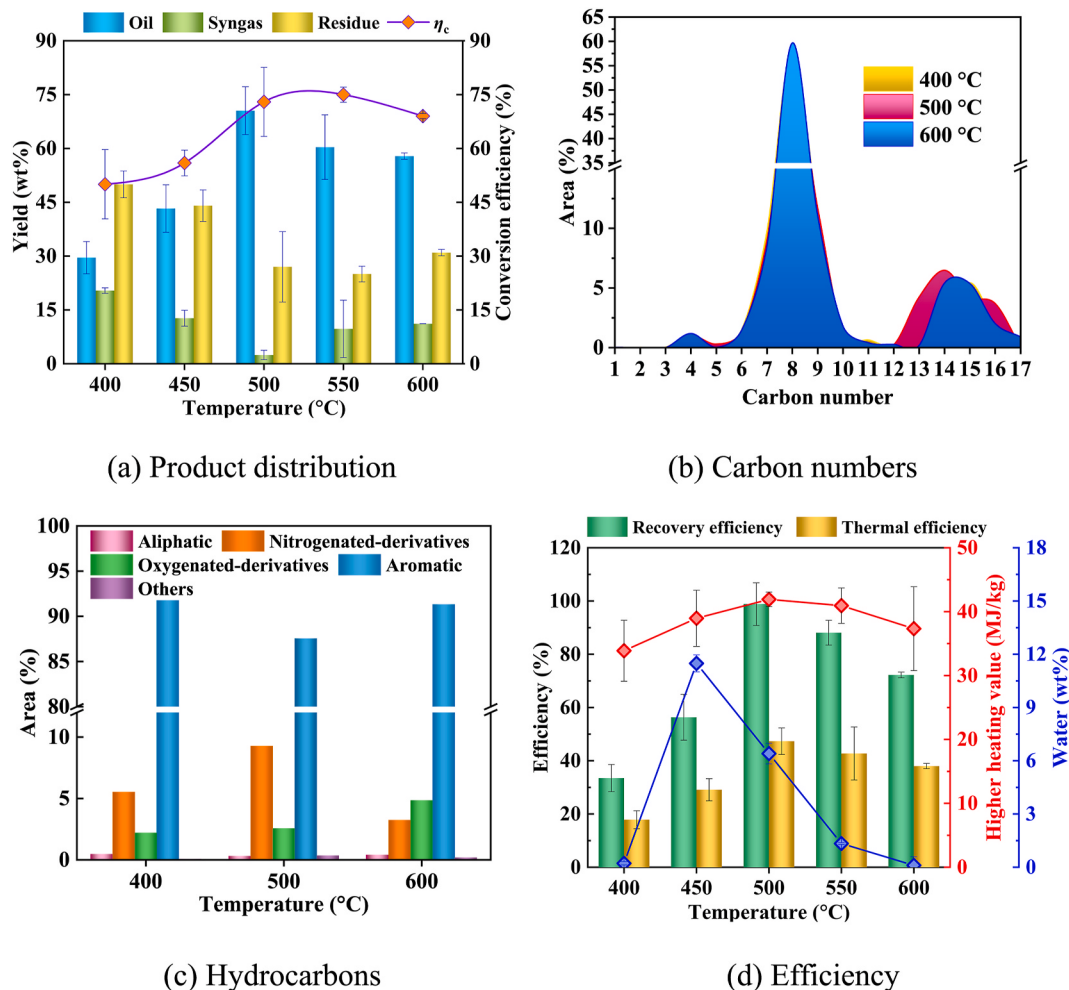


Fig. 6. Effect of different temperatures on microwave-assisted co-pyrolysis of expanded polystyrene and Semen Abutilon seeds.

Zhang et al., 2018). The least negative synergy (-17.68%) was noted at a 2:1 ratio, prompting further investigation into the role of catalysts in mitigating this negative synergy and improving oil yield at this blend proportion. In the case of catalysts, positive synergy values of 10.13 % and 2.73 % were observed using CaO and Al₂O₃, respectively, as represented in Fig. 5 (b), while other catalysts caused negative synergy. These findings are aligned with previous reports of negative synergy in microwave-assisted co-pyrolysis of polystyrene-rice husk blends (Sridevi et al., 2022) and brown coal-corn stover blends (Zhang et al., 2018). Stančin et al. (2022) reported that increasing plastic content in co-pyrolysis can reduce overall synergy due to thermal and chemical incompatibilities which inhibit biomass decomposition. Additionally, feedstock selection and process parameters influence synergy. Higher heating rates and prolonged residence times can promote secondary cracking, shifting product distribution toward gaseous species. For instance, Ephraim et al. (2018) observed negative synergy in co-pyrolysis due to high temperatures favoring secondary reactions, which reduced oil yields.

The synergistic enhancement of major hydrocarbons during the catalytic study is detailed in Table 4. All three catalysts (Na₂CO₃, CaO, and Fe(NO₃)₃·9H₂O) effectively increased the concentration of aromatic hydrocarbons while reducing nitrogenated and oxygenated derivatives. The most significant synergy for enhancing the concentration of aromatic hydrocarbons was observed with CaO (107.34 %), followed by Fe (NO₃)₃·9H₂O (105.47 %) and Na₂CO₃ (101.54 %). Notably, Na₂CO₃ was particularly effective in decreasing oxygenated derivatives, while Fe (NO₃)₃·9H₂O excelled in boosting aliphatic hydrocarbons.

3.4. Effect of temperature on the co-pyrolysis process

The effect of temperature on catalytic co-pyrolysis was investigated using an EPS:SAS blend ratio of 2:1 and 1 g of CaO at five different temperatures: 400, 450, 500, 550, and 600 °C. During this study, the microwave power was kept constant at 660 W. The results obtained from microwave-assisted co-pyrolysis at these temperatures are presented in Fig. 6.

The yields of oil, syngas, and residue obtained from the catalytic co-pyrolysis of EPS and SAS at different temperatures are presented in Fig. 6 (a). As the temperature increased from 400 °C to 600 °C, the oil yield and conversion efficiency initially increased and finally decreased, while the syngas and residue yields exhibited the opposite trend, first decreasing and then increasing. Specifically, the oil yield increased from 29.56 wt% at 400 °C to a maximum of 70.53 wt% at 500 °C, before declining to 57.86 wt% at 600 °C. Syngas yield, residue yield, and conversion efficiency were in the range of 2.45–20.40 wt%, 25.01–49.98 wt%, and 50.02 %–74.99 %, respectively.

At 400 °C (Fig. 6 a), the low oil yield was attributed to insufficient thermal energy to effectively break down the complex molecular structures of both EPS and SAS. At this stage, EPS primarily melted rather than decomposing, producing limited volatiles and forming substantial wax, which contributed to the high residue yield. When the temperature reached 500 °C, the oil yield improved due to accelerated chemical reactions, enhanced thermal decomposition, and increased volatilization of lighter hydrocarbons (Adnan et al., 2015). However, beyond 500 °C, secondary reactions, such as cracking and gasification, became dominant, causing volatile compounds to decompose into syngas rather than condensing into oil (Wang et al., 2022). This shift led to higher residue and non-condensable gas formation. Additionally, prolonged exposure to high temperatures may degrade the basicity and porosity of CaO (Kumagai et al., 2018), further reducing oil yields. This observed oil yield trend is aligned with previous studies (Calero et al., 2023; Zhang et al., 2018).

The carbon number distribution of oil at pyrolysis temperatures of 400 °C, 500 °C, and 600 °C is presented in Fig. 6 (b). GC-MS analysis revealed that hydrocarbons with carbon numbers ranging from C₂ to C₁₇ accounted for 97.99–98.55 area% of the total oil, with C₇–C₉

Table 5
Chemical composition of oil at different temperatures.

Oil component	Formula	Amount (area%)		
		400 °C	500 °C	600 °C
Aromatic hydrocarbons		91.77	87.54	91.32
Benzene	C ₆ H ₆	1.16	0.98	1.18
Toluene	C ₇ H ₈	9.60	8.86	8.32
Styrene	C ₈ H ₈	46.94	42.68	50.52
α-Methylstyrene	C ₉ H ₁₀	8.50	8.07	7.80
Benzene, (1-methylethyl)-	C ₉ H ₁₂	0.77	0.62	0.56
Benzene, 1-propenyl-	C ₉ H ₁₀	0.40	1.00	0.83
Naphthalene	C ₁₀ H ₈	0.37	0.40	0.65
Anthracene	C ₁₄ H ₁₀	0.43	0.46	0.51
Bibenzyl	C ₁₄ H ₁₄	0.70	0.92	0.74
(E)-Stilbene	C ₁₄ H ₁₂	0.71	0.79	0.95
1H-indene, 2-phenyl-	C ₁₅ H ₁₂	0.36	0.39	0.15
Benzene, 1,1'-(1,3-propanediyl)bis-	C ₁₅ H ₁₆	1.23	1.22	0.78
Aliphatic hydrocarbons		0.45	0.30	0.39
1-Heptene	C ₇ H ₁₄	0.04	0.05	0.03
Undecane	C ₁₁ H ₂₄	0.01	0.02	0.01
Dodecane	C ₁₂ H ₂₆	0.01	0.02	0.02
Tetradecane	C ₁₄ H ₃₀	0.02	0.04	0.03
Oxygenated derivatives of hydrocarbons		2.18	2.55	4.84
Ethyl acetate	C ₄ H ₈ O ₂	1.04	0.93	0.88
Acetic acid, butyl ester	C ₆ H ₁₂ O ₂	0.32	0.33	0.27
2-Heptadecanone	C ₁₇ H ₃₄ O	0.15	0.17	0.01
Nitrogenated derivatives of hydrocarbons		5.52	9.26	3.22
Methsuximide	C ₁₂ H ₁₃ NO ₂	0.03	0.04	0.02
Acridine, 9,10-dihydro-	C ₁₃ H ₁₁ N	0.02	0.03	0.02
Hexadecanamide	C ₁₆ H ₃₃ NO	0.01	0.03	0.02
2,3-Diazabicyclo [2.2.1]hept-2-ene,1,4-diphenyl-	C ₁₇ H ₁₆ N ₂	0.10	0.59	0.38
Others		0.06	0.33	0.15
Disulfide, dimethyl	C ₂ H ₆ S ₂	0.01	0.02	–
3-Bromo-5-ethoxy-4-hydroxybenzaldehyde	C ₉ H ₉ BrO ₃	0.01	0.02	0.01

hydrocarbons being the most abundant across all temperatures. At 400 °C, C₈ hydrocarbons dominated the composition (58.70 area%), followed by C₉ (11.39 area%), C₇ (9.76 area%), C₁₅ (5.43 area%), C₁₃ (2.90 area%), and C₁₄ (2.20 area%). When the temperature increased to 500 °C, the distribution showed minor variations. C₈ remained the predominant component, though its contribution decreased slightly to 54.42 area%, while C₉ (11.73 area%), C₇ (8.99 area%), C₁₄ (6.47 area %), and C₁₅ (4.24 area%) constituted the other major fractions. At 600 °C, C₈ hydrocarbons continued to dominate, accounting for 59.67 area% of the total oil. The other major components consisted of C₉ (11.06 area%), C₇ (8.51 area%), and C₁₄ (5.40 area%), while all remaining hydrocarbons collectively accounted for less than 5 area%.

Fig. 6 (c) presents the hydrocarbon group distribution in oil at temperatures of 400, 500, and 600 °C, with detailed subcomponents listed in Table 5. The aromatic hydrocarbons constituted the predominant fraction (87.54–91.77 area%), while aliphatic hydrocarbons showed a minimal fraction (0.30–0.45 area%). The remaining components followed this abundance order: nitrogenated derivatives (3.22–9.26 area%) > oxygenated derivatives (2.18–4.84 area%) > other hydrocarbons (0.06–0.33 area%). The maximum aromatic concentration (91.77 area%) was observed at 400 °C (Fig. 6 c), coinciding with minimal oxygenated and nitrogenated derivatives. This reflects the preferential decomposition of EPS before SAS, as EPS readily forms stable aromatic hydrocarbons at lower temperatures. In contrast, biomass components (e.g., lignin) require higher temperatures (above 400 °C) for effective breakdown (Anshu et al., 2024). During pyrolysis, EPS degraded into smaller aromatic fragments, including styrene, toluene, and xylene (Table 5), which maintained stable phenyl ring structures (Adnan et al., 2015). The non-monotonic temperature dependence of styrene concentration aligns with the previous report (Zhang et al., 2015).

At 500 °C (Fig. 6 c), enhanced biomass decomposition became evident through increased nitrogenated and oxygenated derivatives.

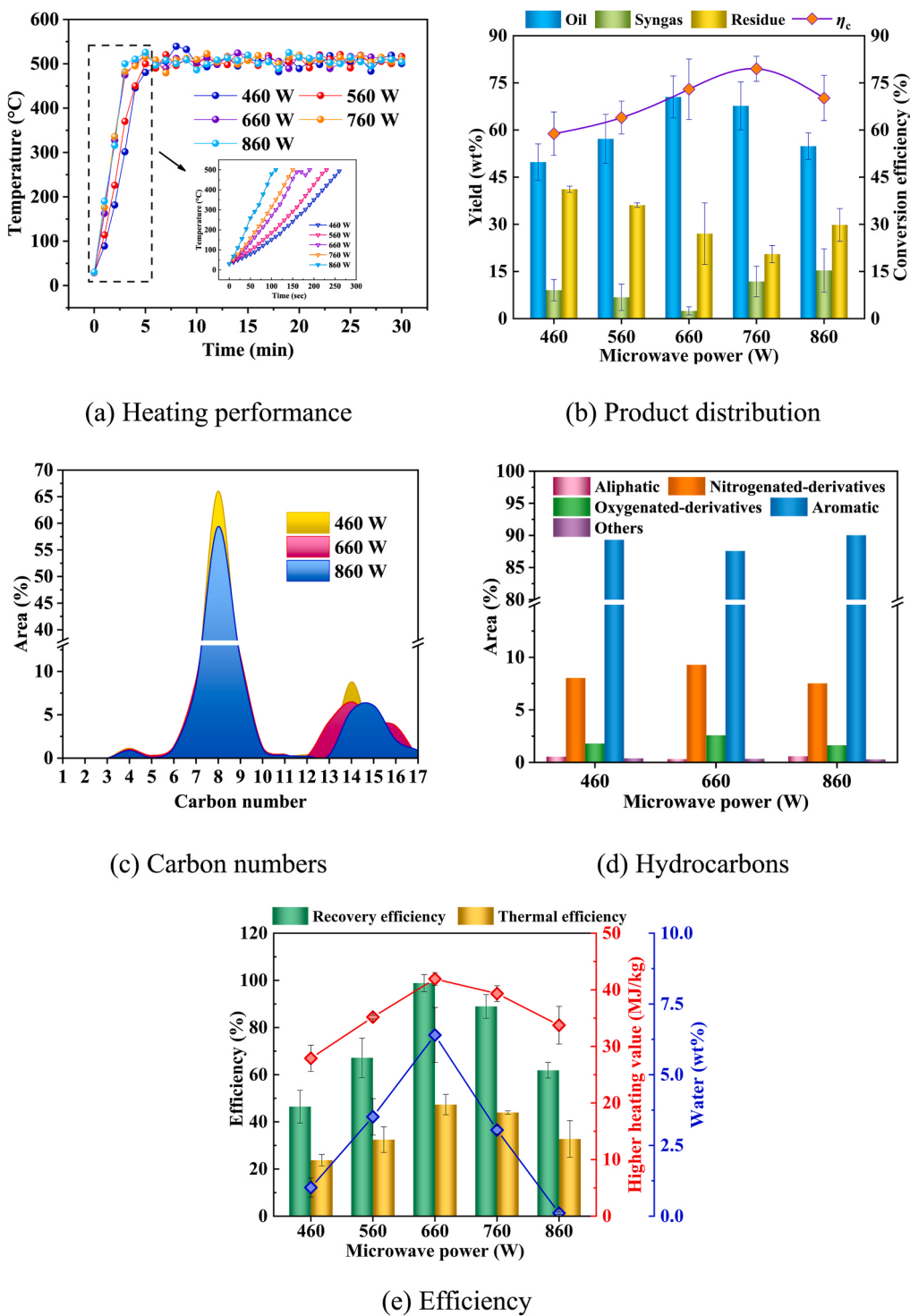


Fig. 7. Effect of different microwave powers on microwave-assisted co-pyrolysis of expanded polystyrene and Semen Abutilon seeds.

The oxygenated derivatives comprised acids, ketones, esters, alcohols, and aldehydes, including phenolic-benzene structures formed through reactions between biomass-derived oxygen and aromatic hydrocarbons (Iftikhar et al., 2019). Upon further temperature increasing to 600 °C, cracking and molecular rearrangement shifted the product distribution, increasing aromatic hydrocarbons while reducing nitrogenated derivatives.

Fig. 6 (d) presents the process efficiencies, HHVs, and water content of oil produced at different temperatures. When the temperature increased from 400 °C to 600 °C, these metrics initially increased and

subsequently decreased. The recovery and thermal efficiencies ranged from 33.48 % to 98.83 % and 17.85 %–47.33 %, respectively, while the HHV and water content spanned 33.88–41.92 MJ/kg and 0.10–11.48 wt %. The optimal process efficiencies occurred at 500 °C, coinciding with the maximum oil yield and HHV at this temperature. At 400 °C, water content was negligible due to incomplete SAS decomposition, but increased at 450 °C as decomposition progressed. Beyond 450 °C, water content declined, likely due to intensified dehydration reactions and thermal dissociation of water molecules into hydrogen and oxygen (Sanahuja-Parejo et al., 2019).

3.5. Effect of microwave power on the co-pyrolysis process

The effect of microwave power on catalytic co-pyrolysis was investigated using an EPS:SAS blend ratio of 2:1 and 1 g of CaO catalyst at five different microwave powers: 460, 560, 660, 760, and 860 W. During this study, the pyrolysis temperature was kept constant at 500 °C. The results obtained from the co-pyrolysis of EPS and SAS at different microwave powers are shown in Fig. 7.

The temperature rise of feedstock at different microwave powers is represented in Fig. 7 (a). At varying microwave powers, the feedstock exhibited different average heating rates, reaching 500 °C at different times. Lower microwave powers required longer exposure to achieve the desired pyrolysis temperature compared to higher microwave powers (Huang et al., 2016; Li et al., 2013). Specifically, average heating rates of 107.4, 124.2, 150.0, 190.2, and 271.2 °C/min were observed at 460, 560, 660, 760, and 860 W, respectively. The corresponding electricity consumption values were 0.145, 0.157, 0.181, 0.176, and 0.149 kWh for these microwave power settings.

The yields of oil, syngas, and residue obtained from the co-pyrolysis of EPS and SAS at different microwave powers are presented in Fig. 7 (b). As the microwave power increased from 460 W to 860 W, the oil yield and conversion efficiency initially rose and then declined. Specifically, the oil yield increased from 9.79 wt% to 70.53 wt% before decreasing to 54.83 wt%, while conversion efficiency varied between 58.83 % and 79.47 %. Conversely, the syngas and residue yields showed an inverse trend, ranging between 2.45 and 15.32 wt% and 20.52–41.15 wt%, respectively. The highest oil yield was achieved at 660 W, identifying this as the optimal microwave power for the process.

At low microwave power (Fig. 7 b), the lower oil yield (9.79 wt%) was due to the slow heating rate and insufficient thermal energy (Jing et al., 2021), which hindered effective feedstock decomposition. Increasing the microwave power initially improved the oil yield by enhancing feedstock degradation efficiency, promoting wax volatilization, and accelerating reaction kinetics (Fan et al., 2023; Kachhadia et al., 2023). However, high microwave power reduced the oil yield due to overheating, secondary reactions, and oil decomposition (Song et al., 2017). At these higher powers, rapid heating limited the time available for efficient conversion, promoting non-condensable gas and residue formation instead of oil. This non-monotonic trend in oil yield with increasing microwave power aligns with previous studies (Li et al., 2013; Song et al., 2017).

The carbon number distribution of oil obtained at microwave powers of 460, 660, and 860 W is presented in Fig. 7 (c). The analysis showed that C₇, C₈, C₉, and C₁₄ hydrocarbons dominated across all microwave power, collectively comprising 81.63–91.36 area% of the total oil composition. At 460 W, the oil was predominantly composed of C₈ hydrocarbons (66.03 area%), followed by C₉ (8.96 area%), C₁₄ (8.78 area%), and C₇ (7.58 area%), with minor contributions (~7.00 area%) from other carbon numbers. When the microwave power was increased to 660 W, the proportion of C₈ hydrocarbons decreased to 54.42 area%, while the distribution of other components followed the order: C₉ (11.73 area%) > C₇ (8.99 area%) > C₁₄ (6.47 area%) > C₁₃ (4.24 area%) > C₁₅ (4.23 area%). At 800 W, the C₈ hydrocarbon concentration rebounded slightly to 59.38 area%, whereas C₁₃ hydrocarbons dropped sharply to 0.33 area%. The proportions of C₇ (8.47 area%), C₉ (11.47 area%), and C₆ (1.20 area%) remained relatively stable. Higher microwave powers led to a slight increase in heavier hydrocarbons, particularly C₁₇₊ (1.95 area%), compared to lower microwave powers.

Fig. 7 (d) presents the hydrocarbon group distribution in the oil at different microwave powers, with detailed subcomponents listed in Table 6. Aromatic hydrocarbons were the dominant fraction, constituting 89.30 area% at 460 W, with styrene alone contributing 56.31 area % of the total aromatics. As microwave power increased to 660 W, the aromatic content decreased to 87.54 area%, likely due to the thermal fragmentation of styrene and its derivatives. However, a subsequent rebound to the 90.01 area% at 860 W suggests the recombination of

Table 6
Chemical composition of oil at different microwave powers.

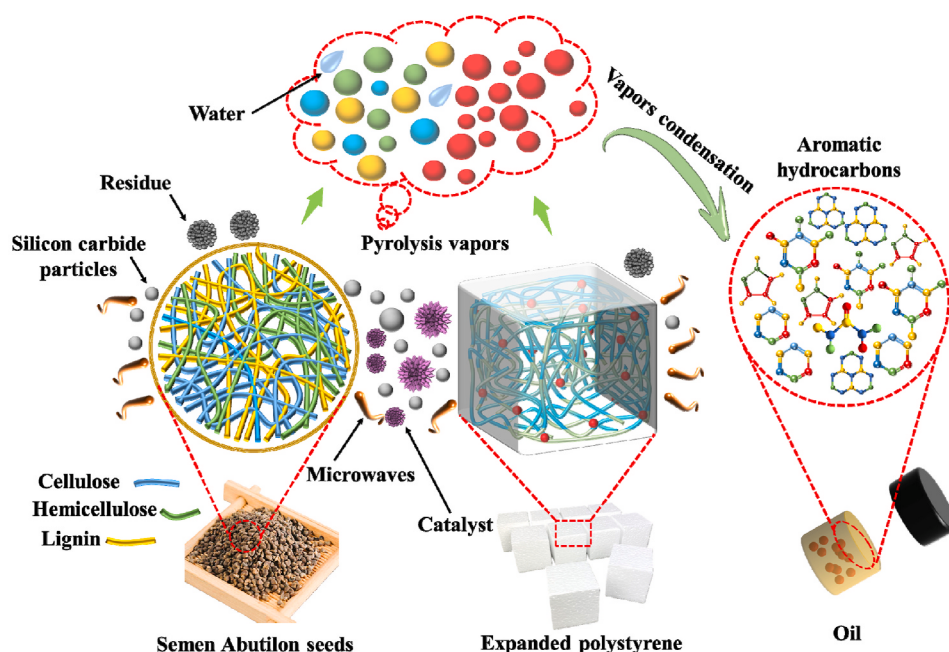
Oil component	Formula	Amount (area%)		
		460 W	660 W	860 W
Aromatic hydrocarbons		89.30	87.54	90.01
Benzene	C ₆ H ₆	0.74	0.98	0.96
Toluene	C ₇ H ₈	7.48	8.86	8.35
Styrene	C ₈ H ₈	56.31	42.68	53.10
α-Methylstyrene	C ₉ H ₁₀	6.46	8.07	8.37
Benzene, (1-methylethyl)-	C ₉ H ₁₂	0.41	0.62	0.64
Benzene, 1-propenyl-	C ₉ H ₁₀	0.46	1.00	0.06
Naphthalene	C ₁₀ H ₈	0.20	0.40	—
Anthracene	C ₁₄ H ₁₀	0.17	0.46	0.24
Bibenzyl	C ₁₄ H ₁₄	0.44	0.92	0.81
(E)-Stilbene	C ₁₄ H ₁₂	0.34	0.79	0.58
1H-indene, 2-phenyl-	C ₁₅ H ₁₂	0.15	0.39	0.25
Benzene, 1,1'-(1,3-propanediyl)bis-	C ₁₅ H ₁₆	0.62	1.22	1.17
Aliphatic hydrocarbons		0.52	0.30	0.57
1-Heptene	C ₇ H ₁₄	0.04	0.05	0.04
Undecane	C ₁₁ H ₂₄	0.02	0.02	0.02
Dodecane	C ₁₂ H ₂₆	0.02	0.02	0.03
Tetradecane	C ₁₄ H ₃₀	0.02	0.04	0.02
Oxygenated derivatives of hydrocarbons		1.77	2.55	1.61
Ethyl acetate	C ₄ H ₈ O ₂	1.01	0.93	0.74
Acetic acid, butyl ester	C ₆ H ₁₂ O ₂	0.33	0.33	0.24
2-Heptadecanone	C ₁₇ H ₃₄ O	0.13	0.17	0.17
Nitrogenated derivatives of hydrocarbons		8.02	9.26	7.51
Methsuximide	C ₁₂ H ₁₃ NO ₂	—	0.04	0.04
Acridine, 9,10-dihydro-	C ₁₃ H ₁₁ N	0.03	0.03	0.02
Hexadecanamide	C ₁₆ H ₃₃ NO	0.01	0.03	0.01
2,3-Diazabicyclo [2.2.1]hept-2-ene,1,4-diphenyl-	C ₁₇ H ₁₆ N ₂	0.24	0.59	0.43
Others		0.37	0.33	0.28
Disulfide, dimethyl	C ₂ H ₆ S ₂	0.01	0.02	0.01
Mepazine	C ₁₉ H ₂₂ N ₂ S	0.15	0.02	0.05

fragmented compounds into more stable aromatic structures. Nitrogenated derivatives, the second most prominent group, reached their maximum concentration (9.26 area%) at 660 W. Oxygenated derivatives (1.61–2.55 area%), primarily comprising acidic and alcoholic compounds, showed a steady decline with increasing microwave power. Aliphatic hydrocarbons remained negligible (<1.00 area%) across all microwave powers, confirming the strong aromatic nature of the oil.

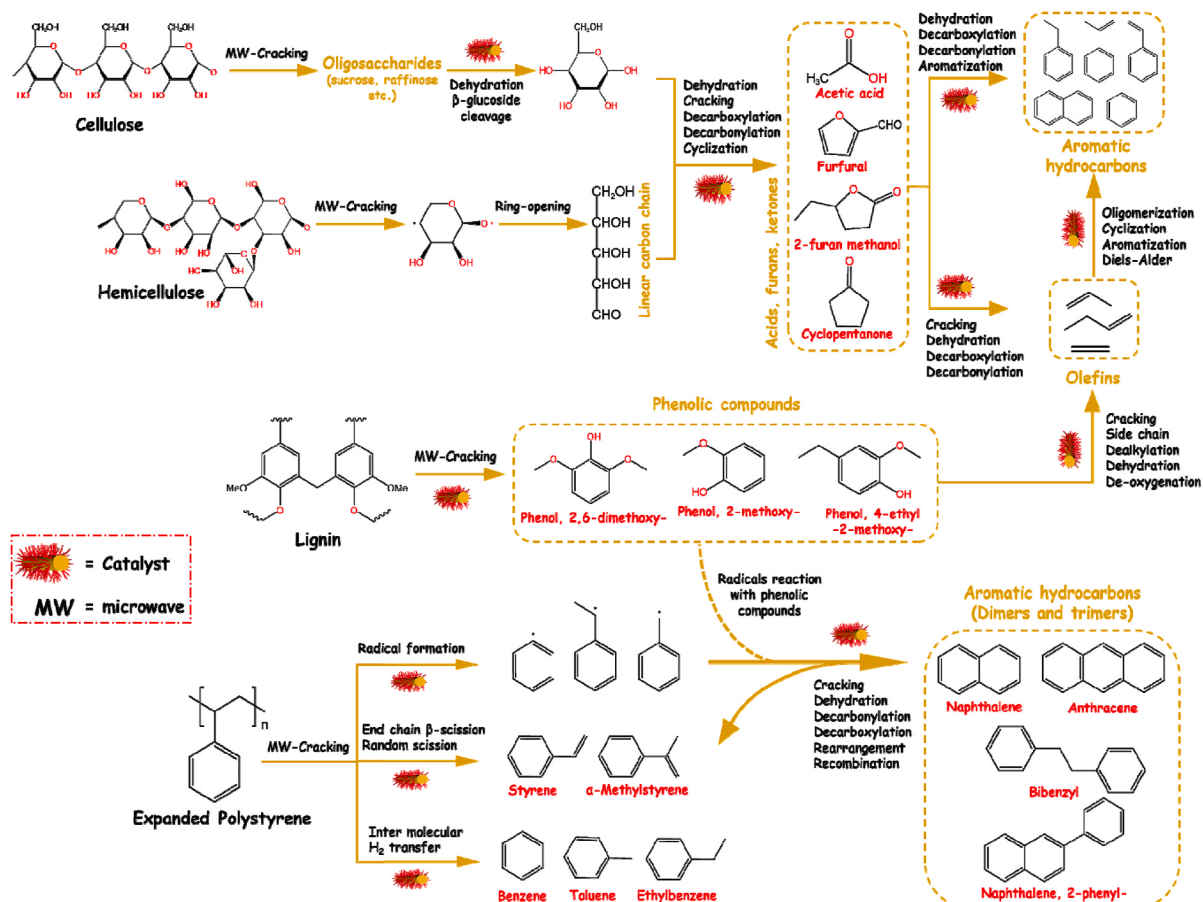
Fig. 7 (e) presents the process efficiencies, HHVs, and water content of oil produced at different microwave powers. These parameters showed a non-linear relationship with microwave power, initially increasing to optimal values before decreasing. At different microwave powers, the thermal and recovery efficiencies ranged from 23.75 % to 47.33 % and 46.44 %–98.32 %, respectively, while the HHV and water contents varied between 27.9 and 41.92 MJ/kg and 0.10–6.40 wt%. Both low and high microwave powers resulted in low oil yields and HHVs, thereby reducing thermal and recovery efficiencies. Additionally, electricity input played a significant role in influencing thermal efficiency (Equation (10)). At low microwave power, the energy consumed by the microwave oven was lower compared to high microwave powers, resulting in decreased thermal efficiency for the co-pyrolysis process.

3.6. Mechanism of catalytic co-pyrolysis for aromatic-enriched oil formation

During catalytic co-pyrolysis, EPS and SAS underwent thermal decomposition, generating volatile vapors that condensed into an aromatic-enriched oil, as shown in Fig. 8 (a). The reaction pathways leading to the formation of aromatic-rich oil were elucidated by integrating mechanistic insights from previous studies on biomass and plastic co-pyrolysis studies (Dai et al., 2020; Lin et al., 2022b; Sanahuja-Parejo et al., 2019; Terry et al., 2023; Zheng et al., 2022), as shown in Fig. 8 (b). The increase in aromatic hydrocarbons can be attributed to catalytic cracking and the synergistic interaction between SAS and EPS, which enhanced deoxygenation. The acid and basic active



(a) Oil formation in catalytic co-pyrolysis



(b) Proposed possible reaction pathways of oil formation

Fig. 8. Mechanism of catalytic co-pyrolysis of EPS and SAS for aromatic-enriched oil formation.

Table 7

Comparison of optimal oil yield and characteristics with previous EPS-biomass co-pyrolysis studies.

Feedstock	Pyrolysis	Conditions	Oil yield (wt%)	Oil composition			Ref.
				Aromatics (area %)	HHV (MJ/kg)	Water (wt%)	
EPS/Palm fronds	Conventional	395 °C, 10:1, -	80.11	73.80	41.56	0.24	Takahashi et al. (2025)
EPS/Semen Abutilon seeds	Microwave	500 °C, 2:1, CaO	70.53	91.77	41.92	0.10–6.40	This study
EPS/Coffee grounds	Conventional	500 °C, 2:1, -	~68.00	87.95	39.66	7.16	Van Nguyen et al. (2021)
EPS/Rubber seeds	Conventional	500 °C, 2:1, -	65.85	49.44	41.10	2.38–11.62	Reshad et al. (2019)
EPS/Fresh water algae	Microwave	600 °C, 1:1, -	~65.00	~80.00	42.20	–	Suriapparao et al. (2022)
		600 °C, 1:1, ZSM-5	~54.00	~5.90	43.70	–	Suriapparao et al. (2022)
EPS/Wheat straw	Microwave	450 °C, 1:1, -	64.90	93.60	41.60	–	Suriapparao et al. (2020)
EPS/Rice husk			61.70	90.70	41.70	–	Suriapparao et al. (2020)
EPS/Pine sawdust	Conventional	500 °C, 2:1, -	63.31	–	39.65	5.04	Van Nguyen et al. (2019)
EPS/Grape seeds	Conventional	550 °C, 2:3, -	62.00	–	39.00	<1.00 ^a	Sanahuja-Parejo et al. (2019)
EPS/Niger seeds	Conventional	550 °C, 1:1, -	61.31	30.70 ^b	32.15	0.00	Shadangi and Mohanty (2015)
EPS/Karanja seeds			60.11	28.58 ^b	38.83	0.00	Shadangi and Mohanty (2015)
EPS/Mahua seeds	Conventional	500 °C, 1:5, -	44.18	31.88 ^c	–	–	Kumar Mishra and Mohanty (2020)
EPS/Coffee grounds	Conventional	500 °C, 1:4, CaO	42.50	1.00 ^d	33.15	3.37	Van Nguyen et al. (2024)
EPS/Sargassum algae	Conventional	600 °C, 2:1, -	~30.00	–	–	–	Kositkanawuth et al. (2017)

^a Water content (<1.00 wt%) in the organic phase, while more water-soluble components condensed in the aqueous phase.^b Calculated as the sum of aromatic hydrocarbons provided in the study.^c Based on NMR analysis.^d Nominalized area% reported in the study.

sites of the catalysts facilitated efficient oxygen removal (Kim et al., 2020; Duan et al., 2017), thereby improving hydrocarbon yields. Oxygenated compounds (acids, furans, alcohols, ketones, and aldehydes) derived from SAS underwent decarboxylation, decarbonylation, and dehydration reactions, converting into less oxygenated or non-oxygenated hydrocarbons (Kim et al., 2020; Zheng et al., 2022). During these processes, water, carbon dioxide, and carbon monoxide were released as by-products, reducing oxygen content in the oil (Terry et al., 2023; Van Nguyen et al., 2024).

EPS primarily decomposed through random scission, β -scission, and intermolecular hydrogen transfer mechanisms (Dogu et al., 2023; Fan et al., 2023). Random scission broke C-C bonds in the polymer chain, producing styrene and oligomers (Sanahuja-Parejo et al., 2019). Meanwhile, β -scission occurred at the β -position relative to a radical site, yielding styrene, α -methylstyrene, and other aromatics (Huang et al., 2020; Park et al., 2020). The β -scission appeared more prominent in the presence of catalysts, increasing styrene yield (Table 3). The dehydrogenation of ethylbenzene may also contribute to the styrene formation (Zhang et al., 2015). Major aromatic hydrocarbons (benzene, toluene, and ethylbenzene) formed through intermolecular hydrogen transfer (Park et al., 2020). Additionally, styrene-derived radicals likely contributed to the aromatic yield (Dogu et al., 2023; Huang et al., 2020).

The key constituents of SAS (cellulose, hemicellulose, and lignin) thermally decomposed to produce primary products (Fig. 8 b). These products migrated through the catalyst's pores, participating in catalytic cracking and deoxygenation to yield secondary products (Lin et al., 2022b; Tian et al., 2022). The cellulose decomposed into oligosaccharides (such as sucrose and raffinose) (Zheng et al., 2022), which further degraded into monosaccharides (e.g., glucose) through catalytic dehydration or the cleavage of β -glucosidic bonds. The hemicellulose yielded monomer radicals that formed open-chain hydrocarbons (Terry et al., 2023). These primary products underwent secondary reactions (cracking, dehydration, and decarboxylation), producing smaller oxygenates such as ketones, furans, and acids (Fig. 8 b) (Tian et al., 2021; Wan Mahari et al., 2022), which were subsequently converted into aromatics and olefins. The concentrations of oxygenated compounds are detailed in Section 3.2. The olefins underwent an aromatization process through atomization, cyclization, and Diels-Alder reactions to form stable aromatic hydrocarbons (Dai et al., 2020). The lignin formed larger oligomers that diffused through catalyst pores (Kim et al., 2020), generating phenolic compounds through cleavage of C-C bonds and

ether linkages (Yu et al., 2019). These phenolics further transformed into aromatics via cyclization and aromatization (Wan Mahari et al., 2022).

A key aspect of co-pyrolysis was the synergistic interaction between EPS-derived radicals and SAS oxygenates, leading to stable aromatic hydrocarbons. Additionally, minor nitrogenated compounds (amines, amides, and nitriles) detected in the oil (Tables 3, 5 and 6) indicate nitrogen presence in SAS. However, the biomass reaction mechanism is a complex process that is difficult to fully elucidate.

3.7. Results comparison with previous studies on EPS and biomass co-pyrolysis

The oil yield and composition obtained under optimized conditions (500 °C, 660 W, CaO catalyst) were compared with previous studies on EPS-biomass co-pyrolysis, as summarized in Table 7. This study achieved a maximum oil yield of 70.53 wt%, characterized by a high HHV of 41.92 MJ/kg, a high aromatic hydrocarbon content (91.77 area%), and a low water content (6.40 wt%), which demonstrates the potential of Semen abutilon seeds as a promising feedstock for co-pyrolysis. The aromatic hydrocarbon yield exceeded most reported values, highlighting the efficacy of CaO in catalyzing deoxygenation and aromatization reactions, which effectively reduce oxygenated compounds and enhance oil quality. The measured HHV range (27.90–42.53 MJ/kg) across different process parameters aligns with reported values for pyrolysis-derived oils (Table 7), with the optimal HHV (42.53 MJ/kg) representing a high-energy-density product suitable for fuel applications. The optimal EPS-to-biomass ratio of 2:1 is consistent with previous findings (Kositkanawuth et al., 2017; Reshad et al., 2019; Van Nguyen et al., 2019, 2021), reinforcing its effectiveness in maximizing oil yield through synergistic interactions. However, Takahashi et al. (2025) reported a higher oil yield (80.11 wt%) using palm fronds at a 10:1 EPS-to-biomass ratio, which can be attributed to the higher volatile matter and lower ash content of palm fronds compared to SAS, as well as the greater plastic proportion in their feedstock. While a high plastic ratio boosts oil yield, it raises concerns about sustainability and product quality, making the 2:1 blend ratio investigated in this study a more balanced and environmentally favorable alternative.

4. Conclusions

This study successfully explored the catalytic co-pyrolysis of SAS and EPS under microwave irradiation. The results showed that an optimal oil yield of 70.53 wt% was achieved under the process conditions of 500 °C, 660 W, and CaO, using an EPS-SAS blend ratio of 2:1. Notably, both CaO and Al₂O₃ catalysts induced a synergistic effect between the feedstocks, enhancing oil yields by 35.56 % and 25.94 %, respectively, compared to non-catalytic conditions (52.02 wt%). The oil produced from SAS pyrolysis alone contained a low proportion of aromatic hydrocarbons (2.79 area%), along with high water content (62.86 wt%) and oxygenated derivatives (74.92 area%). However, catalytic co-pyrolysis improved the oil quality by reducing water content by 85.96 %–99.82 %, decreasing oxygenated derivatives by 93.53 %–98.14 %, and increasing aromatic hydrocarbons by 96.8 %–96.95 %, relative to pyrolysis of SAS alone. The proposed reaction mechanism suggests that EPS acts as a hydrogen donor during catalytic co-pyrolysis, promoting deoxygenation reactions and reducing undesirable oxygenates.

CRediT authorship contribution statement

Faizan Ahmad: Writing – original draft. **Yaning Zhang:** Supervision, Funding acquisition. **Zhihong Liu:** Investigation. **Wenke Zhao:** Validation. **Wei Liu:** Supervision. **Yong Shuai:** Supervision.

Declaration of competing interest

The authors declare that they have no known competing financial interests or personal relationships that could have appeared to influence the work reported in this paper.

Acknowledgements

Financial support was provided by the National Natural Science Foundation of China (52476005), Heilongjiang Province “Double First-class” Discipline Collaborative Innovation Achievement Project (LJGXCG 2023-080), Heilongjiang Provincial Key R&D Program (2023ZX02C05), and Heilongjiang Provincial Key R&D Program “Unveiling the Leader” Project (2023ZXJ02C04).

Data availability

Data will be made available on request.

References

- Adnan, Shah, J., Jan, M.R., 2015. Effect of polyethylene terephthalate on the catalytic pyrolysis of polystyrene: investigation of the liquid products. *J. Taiwan Inst. Chem. Eng.* 51, 96–102.
- Anshu, K., Kenttämaa, H.I., Thengane, S.K., 2024. A comprehensive review on co-pyrolysis of lignocellulosic biomass and polystyrene. *Renew. Sustain. Energy Rev.* 205, 114832.
- Calero, M., Solís, R.R., Muñoz-Batista, M.J., Pérez, A., Blázquez, G., Ángeles Martín-Lara, M., 2023. Oil and gas production from the pyrolytic transformation of recycled plastic waste: an integral study by polymer families. *Chem. Eng. Sci.* 271, 118569.
- Dai, L., Wang, Y., Liu, Y., He, C., Ruan, R., Yu, Z., Jiang, L., Zeng, Z., Wu, Q., 2020. A review on selective production of value-added chemicals via catalytic pyrolysis of lignocellulosic biomass. *Sci. Total Environ.* 749, 142386.
- Dogu, O., Eschenbacher, A., John Varghese, R., Dobbelaere, M., D'hooge, D.R., Van Steenberge, P.H.M., Van Geem, K.M., 2023. Bayesian tuned kinetic monte carlo modeling of polystyrene pyrolysis: unraveling the pathways to its monomer, dimers, and trimers formation. *Chem. Eng. J.* 455, 140708.
- Duan, D., Wang, Y., Dai, L., Ruan, R., Zhao, Y., Fan, L., Tayier, M., Liu, Y., 2017. Ex-situ catalytic co-pyrolysis of lignin and propylene to upgrade bio-oil quality by microwave heating. *Bioresour. Technol.* 241, 207–213.
- Ephraim, A., Pham Minh, D., Lebonnois, D., Peregrina, C., Sharrock, P., Nzhou, A., 2018. Co-pyrolysis of wood and plastics: influence of plastic type and content on product yield, gas composition and quality. *Fuel* 231, 110–117.
- Fan, S., Zhang, Y., Cui, L., Maqsood, T., Nižetić, S., 2023. Cleaner production of aviation oil from microwave-assisted pyrolysis of plastic wastes. *J. Clean. Prod.* 390, 136102.
- Huang, J., Li, X., Meng, H., Tong, H., Cai, X., Liu, J., 2020. Studies on pyrolysis mechanisms of syndiotactic polystyrene using DFT method. *Chem. Phys. Lett.* 747, 137334.
- Huang, Y.F., Chiueh, P., Te, Kuan, W.H., Lo, S.L., 2016. Microwave pyrolysis of lignocellulosic biomass: heating performance and reaction kinetics. *Energy* 100, 137–144.
- Iftikhar, H., Zeeshan, M., Iqbal, S., Muneer, B., Razzaq, M., 2019. Co-pyrolysis of sugarcane bagasse and polystyrene with ex-situ catalytic bed of metal oxides/HZSM-5 with focus on liquid yield. *Bioresour. Technol.* 289, 121647.
- Iliopoulos, E.F., Stefanidis, S.D., Kalogiannis, K.G., Delimitis, A., Lappas, A.A., Triantafyllidis, K.S., 2012. Catalytic upgrading of biomass pyrolysis vapors using transition metal-modified ZSM-5 zeolite. *Appl. Catal., B* 127, 281–290.
- Jing, X., Dong, J., Huang, H., Deng, Y., Wen, H., Xu, Z., Ceylan, S., 2021. Interaction between feedstocks, absorbers and catalysts in the microwave pyrolysis process of waste plastics. *J. Clean. Prod.* 291, 125857.
- Kachadiya, K., Patel, D., Vijaybhai, G.J., Raghuvaran, P., Surya, D.V., Dharaskar, S., Kumar, G.P., Reddy, B.R., Remya, N., Kumar, T.H., Basak, T., 2023. Conversion of waste polystyrene into valuable aromatic hydrocarbons via microwave-assisted pyrolysis. *Environ. Sci. Pollut. Res.* 31 (46), 57509–57522.
- Kim, J.Y., Moon, J., Lee, J.H., Jin, X., Choi, J.W., 2020. Conversion of phenol intermediates into aromatic hydrocarbons over various zeolites during lignin pyrolysis. *Fuel* 279, 118484.
- Kositkanawut, K., Bhatt, A., Sattler, M., Dennis, B., 2017. Renewable energy from waste: investigation of co-pyrolysis between sargassum macroalgae and polystyrene. *Energy Fuels* 31, 5088–5096.
- Kulakovskaya, A., Wiprachtiger, M., Knoeri, C., Bening, C.R., 2023. Integrated environmental-economic circular economy assessment: application to the case of expanded polystyrene. *Resour. Conserv. Recycl.* 197, 107069.
- Kumagai, S., Yamasaki, R., Kameda, T., Saito, Y., Watanabe, A., Watanabe, C., Teramae, N., Yoshioka, T., 2018. Aromatic hydrocarbon selectivity as a function of CaO basicity and aging during CaO-catalyzed PET pyrolysis using tandem μ-reactor-GC/MS. *J. Chem. Eng.* 332, 169–173.
- Kumar Mishra, R., Mohanty, K., 2020. Co-pyrolysis of waste biomass and waste plastics (polystyrene and waste nitrile gloves) into renewable fuel and value-added chemicals. *Carbon Resour. Convers.* 3, 145–155.
- Li, L., Ma, X., Xu, Q., Hu, Z., 2013. Influence of microwave power, metal oxides and metal salts on the pyrolysis of algae. *Bioresour. Technol.* 142, 469–474.
- Lin, F., Xu, M., Ramasamy, K.K., Li, Z., Klinger, J.L., Schaidle, J.A., Wang, H., 2022a. Catalyst deactivation and its mitigation during catalytic conversions of biomass. *ACS Catal.* 12 (21), 13555–13559.
- Lin, X., Zhang, Z., Wang, Q., Sun, J., 2022b. Interactions between biomass-derived components and polypropylene during wood-plastic composite pyrolysis. *Biomass Conv. Bioref.* 12, 3345–3357.
- Mordor Intelligence, 2025. Expanded polystyrene market size & share analysis - growth trends & forecasts (2025 - 2030). Retrieved from. <https://www.mordorintelligence.com/industry-reports/global-expanded-polystyrene-eps-market-industry>.
- Nanda, S., Berruti, F., 2021. Thermochemical conversion of plastic waste to fuels: a review. *Environ. Chem. Lett.* 19 (1), 123–148.
- Ochoa, A., Bilbao, J., Gayubo, A.G., Castaño, P., 2020. Coke formation and deactivation during catalytic reforming of biomass and waste pyrolysis products: a review. *Renew. Sustain. Energy Rev.* 119, 109600.
- Pan, X., Wu, Y., Li, T., Lan, G., Shen, J., Yu, Y., Xue, P., Chen, D., Wang, M., Fu, C., 2023. A study of co-pyrolysis of sewage sludge and rice husk for syngas production based on a cyclic catalytic integrated process system. *Renew. Energy* 215, 118946.
- Park, K.B., Jeong, Y.S., Guzelciftci, B., Kim, J.S., 2020. Two-stage pyrolysis of polystyrene: pyrolysis oil as a source of fuels or benzene, toluene, ethylbenzene, and xylenes. *Appl. Energy* 259, 114240.
- Reshad, A.S., Tiwari, P., Goud, V.V., 2019. Thermal and co-pyrolysis of rubber seed cake with waste polystyrene for bio-oil production. *J. Anal. Appl. Pyrolysis* 139, 333–343.
- Rillig, M.C., Lehmann, A., 2020. Microplastic in terrestrial ecosystems. *Science* 368 (6498), 1430–1431.
- Sanahuja-Parejo, O., Veses, A., Navarro, M.V., López, J.M., Murillo, R., Callén, M.S., García, T., 2019. Drop-in biofuels from the co-pyrolysis of grape seeds and polystyrene. *J. Chem. Eng.* 377, 120246.
- Sebestyén, Z., Barta-Rajnai, E., Bozi, J., Blazsó, M., Jakab, E., Miskolczi, N., Sójá, J., Czéghény, Z., 2017. Thermo-catalytic pyrolysis of biomass and plastic mixtures using HZSM-5. *Appl. Energy* 207, 114–122.
- Shadangi, K.P., Mohanty, K., 2015. Co-pyrolysis of karanja and niger seeds with waste polystyrene to produce liquid fuel. *Fuel* 153, 492–498.
- Song, Z., Yang, Y., Sun, J., Zhao, X., Wang, W., Mao, Y., Ma, C., 2017. Effect of power level on the microwave pyrolysis of tire powder. *Energy* 127, 571–580.
- Sridevi, V., Suriaaparaao, D.V., Tukarambai, M., Terapalli, A., Ramesh, P., Sankar Rao, C., Gautam, R., Moorthy, J.V., Suresh Kumar, C., 2022. Understanding of synergy in non-isothermal microwave-assisted in-situ catalytic co-pyrolysis of rice husk and polystyrene waste mixtures. *Bioresour. Technol.* 360, 127589.
- Stancin, H., Šafář, M., Ružicková, J., Mikulčíč, H., Raclavská, H., Wang, X., Duić, N., 2022. Influence of plastic content on synergistic effect and bio-oil quality from the co-pyrolysis of waste rigid polyurethane foam and sawdust mixture. *Renew. Energy* 196, 1218–1228.
- Sun, S., Guo, J., Chen, X., 2021. Biodiesel preparation from Semen abutili (Abutilon theophrasti medic.) seed oil using low-cost liquid lipase Eversa® transform 2.0 as a catalyst. *Ind. Crops Prod.* 169, 113643.
- Suriaparaao, D.V., Hemanth Kumar, T., Reddy, B.R., Yerrayya, A., Srinivas, B.A., Sivakumar, P., Prakash, S.R., Sankar Rao, C., Sridevi, V., Desinghu, J., 2022. Role of ZSM5 catalyst and char susceptor on the synthesis of chemicals and hydrocarbons

- from microwave-assisted in-situ catalytic co-pyrolysis of algae and plastic wastes. *Renew. Energy* 181, 990–999.
- Suriapparao, D.V., Yerraya, A., Nagababu, G., Guduru, R.K., Kumar, T.H., 2020. Recovery of renewable aromatic and aliphatic hydrocarbon resources from microwave pyrolysis/co-pyrolysis of agro-residues and plastics wastes. *Bioresour. Technol.* 318, 124277.
- Takahasi, A.P.D., Mansur, D., Prasetyo, W.D., Simanungkalit, S.P., Purba, W.L.I., Rizal, W.A., Sarwono, A., Iskandar, Y.A., 2025. Optimization of liquid fuel production from co-pyrolysis of oil palm fronds and expanded polystyrene using response surface methodology. *Case Stud. Chem. Environ. Eng.* 11, 101074.
- Terry, L.M., Wee, M.X.J., Chew, J.J., Khaerudini, D.S., Darsono, N., Aqsha, A., Saptoyo, A., Sunarso, J., 2023. Catalytic co-pyrolysis of oil palm trunk and polypropylene with Ni-Mo/TiO₂ and Ni/Al₂O₃: oil composition and mechanism. *Environ. Res.* 224, 115550.
- Tian, B., Xu, L., Jing, M., Liu, N., Tian, Y., 2021. A comprehensive evaluation on pyrolysis behavior, kinetics, and primary volatile formation pathways of rice husk for application to catalytic valorization. *Fuel Process. Technol.* 214, 106715.
- Tian, H., Chen, L., Huang, Z., Cheng, S., Yang, Y., 2022. Increasing the bio-aromatics yield in the biomass pyrolysis oils by the integration of torrefaction/deoxygenation pretreatment and catalytic fast pyrolysis with a dual catalyst system. *Renew. Energy* 187, 561–571.
- Van Nguyen, Q., Choi, Y.S., Choi, S.K., Jeong, Y.W., Kwon, Y.S., 2019. Improvement of bio-crude oil properties via co-pyrolysis of pine sawdust and waste polystyrene foam. *J. Environ. Manag.* 237, 24–29.
- Van Nguyen, Q., Choi, Y.S., Choi, S.K., Jeong, Y.W., Han, S.Y., 2021. Co-pyrolysis of coffee-grounds and waste polystyrene foam: synergistic effect and product characteristics analysis. *Fuel* 292, 120375.
- Van Nguyen, Q., Choi, Y.S., Jeong, Y.W., Han, S.Y., Choi, S.K., 2024. Catalytic co-pyrolysis of coffee-grounds and waste polystyrene foam by calcium oxide in bubbling fluidized bed reactor. *Renew. Energy* 224, 120124.
- Varma, A.K., Lal, N., Rathore, A.K., Katiyar, R., Thakur, L.S., Shankar, R., Mondal, P., 2021. Thermal, kinetic and thermodynamic study for co-pyrolysis of pine needles and styrofoam using thermogravimetric analysis. *Energy* 218, 119404.
- Wang, F., Zhang, Y., Zeng, X., Yue, J., Zhang, G., Hu, D., Haruna Adamu, M., Lai, X., Xu, G., 2022. Insight into tar thermal cracking and catalytic cracking by char: characteristics and kinetics. *Fuel* 326, 124929.
- Wang, Q., Zhang, X., Sun, S., Wang, Z., Cui, D., 2020. Effect of CaO on pyrolysis products and reaction mechanisms of a corn stover. *ACS Omega* 5 (18), 10276–10287.
- Wan Mahari, W.A., Awang, S., Zahariman, N.A.Z., Peng, W., Man, M., Park, Y.K., Lee, J., Sonne, C., Lam, S.S., 2022. Microwave co-pyrolysis for simultaneous disposal of environmentally hazardous hospital plastic waste, lignocellulosic, and triglyceride biowaste. *J. Hazard Mater.* 423, 127096.
- Yu, D., Hui, H., Li, S., 2019. Two-step catalytic co-pyrolysis of walnut shell and LDPE for aromatic-rich oil. *Energy Convers. Manag.* 198, 111816.
- Zhang, L., Wu, Z., Nelson, N.C., Sadow, A.D., Slowing, I.I., Overbury, S.H., 2015. Role of CO₂ as a soft oxidant for dehydrogenation of ethylbenzene to styrene over a high-surface-area ceria catalyst. *ACS Catal.* 5 (11), 6426–6435.
- Zhang, Y., Fan, L., Liu, S., Zhou, N., Ding, K., Peng, P., Anderson, E., Addy, M., Cheng, Y., Liu, Y., Li, B., Snyder, J., Chen, P., Ruan, R., 2018. Microwave-assisted co-pyrolysis of brown coal and corn stover for oil production. *Bioresour. Technol.* 259, 461–464.
- Zheng, Y., Wang, J., Wang, D., Zheng, Z., 2022. Advanced catalytic upgrading of biomass pyrolysis vapor to bio-aromatics hydrocarbon: a review. *Appl. Energy Combust. Sci.* 10, 100061.